

## RESEARCH ARTICLE

10.1029/2022JD037860

## Key Points:

- High resolution WRF-Chem modeling reproduces observed spatiotemporal variability of NO<sub>2</sub> and O<sub>3</sub> during sea breezes in the Greater Boston area
- Model results suggest high O<sub>3</sub> pollution and NO<sub>2</sub> column spatial variability associated with sea breezes is not captured by current monitoring
- Monitoring coastal urban air quality requires customized strategies with high-resolution modeling and well-allocated observations

## Supporting Information:

Supporting Information may be found in the online version of this article.

## Correspondence to:

B. Wang,  
[bowang@bu.edu](mailto:bowang@bu.edu)

## Citation:






Wang, B., Geddes, J. A., Adams, T. J., Lind, E. S., McDonald, B. C., He, J., et al. (2023). Implications of sea breezes on air quality monitoring in a coastal urban environment: Evidence from high resolution modeling of NO<sub>2</sub> and O<sub>3</sub>. *Journal of Geophysical Research: Atmospheres*, 128, e2022JD037860. <https://doi.org/10.1029/2022JD037860>

Received 14 SEP 2022  
Accepted 12 APR 2023

## Author Contributions:

**Conceptualization:** Bo Wang, Jeffrey A. Geddes, Gabriele G. Pfister  
**Data curation:** Jeffrey A. Geddes  
**Formal analysis:** Bo Wang, Jeffrey A. Geddes  
**Funding acquisition:** Jeffrey A. Geddes  
**Investigation:** Bo Wang, Jeffrey A. Geddes  
**Methodology:** Bo Wang, Jeffrey A. Geddes, Dan Li  
**Project Administration:** Jeffrey A. Geddes  
**Resources:** Bo Wang, Jeffrey A. Geddes, Taylor J. Adams, Elena S. Lind, Brian C. McDonald, Jian He, Colin Harkins, Dan Li, Gabriele G. Pfister  
**Supervision:** Jeffrey A. Geddes  
**Visualization:** Bo Wang

# Implications of Sea Breezes on Air Quality Monitoring in a Coastal Urban Environment: Evidence From High Resolution Modeling of NO<sub>2</sub> and O<sub>3</sub>

Bo Wang<sup>1</sup> , Jeffrey A. Geddes<sup>1</sup> , Taylor J. Adams<sup>1</sup>, Elena S. Lind<sup>2,3</sup>, Brian C. McDonald<sup>4</sup>, Jian He<sup>4,5</sup>, Colin Harkins<sup>4,5</sup> , Dan Li<sup>1</sup> , and Gabriele G. Pfister<sup>6</sup> 

<sup>1</sup>Department of Earth and Environment, Boston University, Boston, MA, USA, <sup>2</sup>Department of Electrical and Computer Engineering, Virginia Tech, Blacksburg, VA, USA, <sup>3</sup>Now at NASA Goddard Space Flight Center, Greenbelt, MD, USA, <sup>4</sup>Chemical Sciences Laboratory, NOAA Earth System Research Laboratories, Boulder, CO, USA, <sup>5</sup>Cooperative Institute for Research in Environmental Sciences, University of Colorado, Boulder, CO, USA, <sup>6</sup>Atmospheric Chemistry Observations and Modeling Laboratory, NCAR, Boulder, CO, USA

**Abstract** Coastal urban environments face unique challenges associated with air quality-meteorology interactions. In this study, high resolution chemical transport modeling over the Greater Boston area was performed to improve our understanding of sea breezes impacts on the spatiotemporal variability of primary and secondary pollutants. We perform WRF-Chem simulations at 3 km resolution over June 22 to 10 July 2019 (a period that included 10 sea breeze occurrences), and use Pandora tropospheric NO<sub>2</sub> column, surface air quality monitoring, and vertical meteorological aircraft profiles for evaluation. The model generally reproduces observed spatiotemporal variability of air pollution during sea breezes well. Tropospheric columns of NO<sub>2</sub> predicted by the model and observed by the Pandora instrument show that sea breezes are associated with rapid increases and steep gradients in tropospheric NO<sub>2</sub> and confirm accumulation of local primary emissions. Spatial heterogeneity in tropospheric NO<sub>2</sub> is strongly governed by inland penetration lengths of the sea breeze front. Process diagnostics show that three sea-breeze days where O<sub>3</sub> observations recorded hourly concentrations >70 ppb have both efficient net chemical O<sub>3</sub> production in the boundary layer (>10 ppb/hr) and rapid O<sub>3</sub> convergence in the near-surface convergence zone (>20 ppb/hr). During sea breezes, interactions between photochemistry, the convergence zone inland penetration, and urban NO<sub>x</sub> titration effects, contribute to strong heterogeneity and high O<sub>3</sub> inland that is not captured by the current monitoring network. We discuss monitoring needs and model applications for the sea breeze scenarios, with broad implications for air quality monitoring in coastal urban environments.

**Plain Language Summary** The sea breeze is a local meteorological system that brings air from the sea over the land during the day. In areas that usually experience offshore winds, this means the system can recirculate early morning pollutant emissions back onshore later in the day. Understanding the behavior of air pollutants in coastal urban environments is essential for air quality management, but land-sea breeze circulations are characterized by fine scale features and rapid changes in pollution levels that pose challenges for traditional monitoring and satellite retrievals. In the Greater Boston area, we use highly resolved information from a regional chemical transport model combined with observational assets to examine pollutant behavior and model performance. We find new evidence of underestimated regional ozone pollution and nitrogen dioxide column spatial variability associated with sea breezes. This variability is governed by how far the sea breeze penetrates inland, but is also affected by interactions between chemistry and atmospheric dynamic that are not well captured by current monitoring and coarse resolution models. Our results provide valuable insights for future ground-based and satellite remote sensing monitoring, highlighting that customized strategies for monitoring coastal urban air quality are required from high-resolution models constrained by carefully allocated observations.

## 1. Introduction

The sea breeze system (and its lake/bay breeze counterparts) is driven by thermally induced mesoscale pressure gradients and consists of spatiotemporally nested phenomena (Miller et al., 2003). Past studies have revealed that the sea breeze system plays a distinct role in the spatiotemporal distribution of primary and secondary air pollutants in coastal urban environments (Caicedo et al., 2021; Ding et al., 2004; Geddes et al., 2021; Kitada

**Writing – original draft:** Bo Wang  
**Writing – review & editing:** Bo Wang, Jeffrey A. Geddes, Taylor J. Adams, Elena S. Lind, Brian C. McDonald, Jian He, Colin Harkins, Dan Li, Gabriele G. Pfister

et al., 1986; Kotsakis et al., 2022; Loughner et al., 2011; Martins et al., 2012; Wentworth et al., 2015). Spatially, the sea breeze system can introduce sharp spatial gradients and chemical fronts. For example, multi-platform measurements in field campaigns have captured significant ozone ( $O_3$ ) gradients over the land-water interface (Stanier et al., 2021; Sullivan et al., 2019; J. Zhang et al., 2020). Temporally, sea breezes can cause rapid changes of local air pollutants, sometimes up to unhealthy levels, and can indirectly impact air quality in regions downwind of metropolitan emission sources. For example, Loughner et al. (2014) combined observations and model output to show that the inland-penetrated bay-breeze convergence zone can exacerbate surface  $O_3$  pollution levels near the Chesapeake Bay. Stauffer et al. (2015) showed that bay breezes worsen poor air quality that persists into the late evening hours in that area, and cause large horizontal and vertical gradients of  $O_3$ . Developing air quality models that can sufficiently resolve these dynamics and associated chemistry, along with consistent monitoring, is therefore a high priority for air quality management in coastal urban regions, where the significant portion of the world's population and emission sources are concentrated.

Regional chemical transport models have been widely used for land-sea breeze simulations in field campaigns and research activities (Abdi-Oskouei et al., 2020; Blaylock et al., 2017; Caicedo et al., 2019). It is challenging to reproduce both sea breeze transport and impacts on air pollution well, as model performance can be affected by many different factors. Chief among these may be the model resolution, due to the importance of representing the mesoscale and localized features presented by sea breezes. Loughner et al. (2011) examined the effects of varying horizontal resolution on the development of the Chesapeake Bay breeze, and they found that simulations with 4.5 km or finer resolution produce an earlier onset time and stronger bay breeze than with the coarser resolution at 13.5 km. Colby (2004) shows that high-resolution grids (e.g., 4 km) are able to resolve realistic details in the sea-breeze flow along the eastern New England coast. Judd et al. (2019) speculated that a model with a 12 km resolution might not be enough to represent an accurate shape factor for a priori assumptions for the sea breeze environment over Los Angeles Basin. Another critical factor is the accuracy of anthropogenic emissions input. Especially in urban areas, overestimated mobile sources of nitrogen oxides ( $NO_x$ ) could significantly affect the model accuracy (Anderson et al., 2014).

Accurate high-resolution modeling of sea breeze cases can inform routine and real-time monitoring networks. Longstanding challenges include the sparse ground-based monitoring available for global to regional assessment of spatial heterogeneity in air pollution, and the insufficient temporal snapshots (and spatial resolution) from traditional satellite-based sensors. The latest generation of geostationary satellite instruments will provide unprecedented spatiotemporal resolution for pollution monitoring within urban areas (e.g., TEMPO (Zoogman et al., 2017) and GEMS (Kim et al., 2020)). However, challenges associated with air quality-meteorology interactions in coastal urban regions could give rise to inaccuracies in the chemical inputs required by the satellite retrievals. The difficulties are partly due to insufficient model or geophysical input resolution in representing sea breeze transport and spatiotemporal variability of pollutants (Geddes et al., 2021; Goldberg et al., 2017; Judd et al., 2019). In addition, column measurements alone are challenging to interpret during poor air quality episodes in coastal regions (Thompson et al., 2019). Understanding the small-scale variability from surface to column scales in complex meteorological conditions, especially during sea breezes commonly experienced in coastal regions, is needed to improve satellite-inferred surface-level air quality conditions and to examine the long-term trends (Geddes et al., 2016).

The Boston area is on the cusp of violating the U.S. Environment Protection Agency (EPA) air quality standard for  $O_3$  (Geddes et al., 2021), especially if EPA revisits current air quality standards (based on a daily maximum 8-hr average of 70 ppb) for a lower-level threshold. Furthermore, Rieder et al. (2015) demonstrated that while regional emission controls should effectively reduce summertime  $O_3$  pollution in the eastern United States, increasing  $O_3$  exceedances for the Greater Boston region are projected under present-day emissions in a moderate climate-warming scenario. Therefore, understanding and monitoring pollution is necessary to inform effective outcomes of emission control policy and public health information in the area. Across the Greater Boston area, Davis et al. (1890) documented one of the earliest meteorological observation records for the sea breeze: the most obvious sea breeze events (excluding the farther-reaching synoptic easterly wind conditions), penetrate inland from Boston up to 20 to 25 miles (i.e., 32–40 km). This penetration distance is beyond the coverage of current routine  $NO_2$  and  $O_3$  monitoring networks and leaves a gap in air pollution information there. Using vertical temperature and dew point data in Boston, Barbato (1978) showed that site conditions and urban form alter the characteristics of the Boston sea breeze with inland penetration noted up to ~30 km. Studies have also investigated the influence of meteorology, coastal boundary layer processes, and topography on Northern New

England pollution episodes, including the impact of plumes being transported from the metropolitan Boston area (Angevine et al., 2004; Darby et al., 2007; Mao & Talbot, 2004). However, the role of sea breezes in the distribution of pollution within the city of Boston itself has not been the focus of these studies. More recently, a climatological analysis of surface observations (Geddes et al., 2021) showed substantial  $O_x$  ( $= NO_2 + O_3$ ) gradients of over 30 ppb across the urban Boston area that are uniquely observed during sea breezes. The study further highlighted the importance of high-resolution chemical transport modeling for local satellite retrieval development in coastal urban environments. In the Greater Boston area, there is a lack of new atmospheric chemistry modeling at the scale required to resolve sea breeze features, interpret these gradients in space and time, and help understand the full impact of the sea breeze's inland penetration on air pollution.

Prompted by previous research and current knowledge gaps, this study aims to investigate the following questions: Can high-resolution ( $\sim 3$  km) modeling reproduce observed patterns (spatiotemporal variability) in air pollution associated with sea breezes in the greater Boston area, and what factors impact the accuracy in simulating sea breeze onset and evolution?

How does the modeling inform spatiotemporal variability in air pollution that may not be captured by current monitoring, and what process-level insight can be obtained to understand this variability? What are the implications for new ground-based monitoring strategies and remote sensing measurements?

To answer these questions, we perform high-resolution modeling with online chemistry over the Boston area for the summer of 2019. The simulation covers multiple sea-breeze and non-sea-breeze days to derive representative conclusions for these various conditions. We use multi-scale observations to evaluate model performance, including surface monitoring networks, vertical profiles, and ground-based remote sensing observations. For the first time, we use Pandora observations on the Boston University (BU) campus in a model evaluation over the urban Boston area, which can provide additional insights for future geostationary monitoring of pollution. We analyze the model spatiotemporal distribution and hotspots of pollution, and diagnose processes that contribute especially to high ozone during sea breezes. We show that our model simulations have broad implications for new ground-based monitoring strategies and remote sensing measurements in coastal urban environments.

## 2. Data and Methods

### 2.1. Study Area and Time Period

Our modeling focuses on several weeks during the summer, which is known to have frequent sea breeze days in Boston (Geddes et al., 2021). We choose a study time period of June 22 to 10 July 2019, characterized by a comparable number of sea-breeze and non-sea-breeze days. Figure 1 shows the study area and observation stations. Vertical meteorological profiles (Section 2.2.3) are observed at Logan Airport, and a Pandora (Section 2.2.1) is deployed in the urban region on the BU campus. The figure also shows the locations of surface air quality monitoring (Section 2.2.2) collected by the Massachusetts Department of Environmental Protection (MassDEP), as well as the locations of other surface meteorological measurements (Section 2.2.3) used in this study. Table S1 in Supporting Information S1 shows the latitude, longitude, altitude, height of sensors, and site environment of all the stations used in this study.

### 2.2. Multi-Platform Measurements

#### 2.2.1. Pandora

The ground-based Pandora spectrometer system determines column integrated amounts of trace gases in the atmosphere using differential optical absorption spectroscopy. This work uses the direct-sun Pandora observations at the BU site at an elevation of  $\sim 30$  m. Pandora's slant  $NO_2$  columns are retrieved using a spectral fitting algorithm (Cede, 2017), which are then converted to a vertical column using an air mass factor which is approximately  $AMF = \secant(\text{Solar Zenith Angle})$ . Direct-sun  $NO_2$  columns produced by Pandora have a clear sky nominal accuracy of 0.1 DU in the vertical column (Herman et al., 2009). The separation of stratospheric and tropospheric columns from the Pandora total column measurement is described in detail elsewhere (Adams et al., 2023). Briefly, an 8-day moving average of GEOS-CF stratospheric  $NO_2$  diurnal variability is scaled with TROPOMI-derived stratospheric  $NO_2$  at its overpass time. This calculated diurnal stratospheric  $NO_2$  column is separated from Pandora total  $NO_2$  column measurements. The quality-filtered Pandora observations are sampled to 5 min. BU Pandora data from June 22 to 10 July 2019 are used in this study.

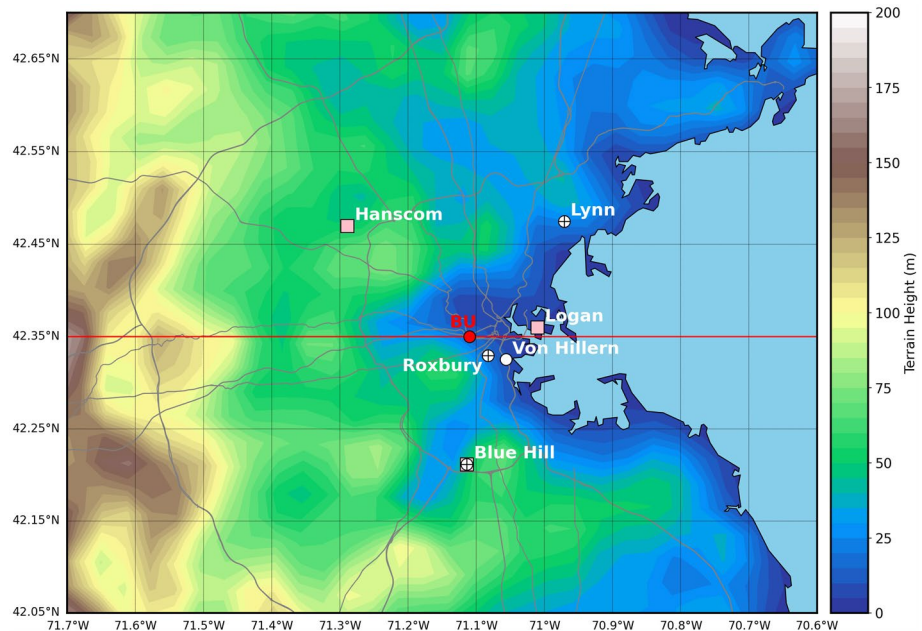


**Figure 1.** Map of the study area in Greater Boston and terrain height (the entire model domain is shown in Figure S1 in Supporting Information S1). The red dot denotes the location of BU Pandora. The white circles denote the MassDEP air monitoring sites for NO<sub>2</sub> (Lynn, Roxbury, Von Hillern, Blue Hill) used in this study, where the plus symbol denotes sites with collocated O<sub>3</sub> observations (Lynn, Roxbury, Blue Hill). The pink squares denote surface wind observations (Logan Airport, Blue Hill, Hanscom). AMDAR profiles are also located at the Logan Airport site. The red line indicates the cross section across the BU Pandora station used for a later Figure.

### 2.2.2. Ambient Air Quality Monitoring

Hourly in-situ observations of ground-level NO<sub>2</sub> and O<sub>3</sub> are retrieved from the Air Quality System repository at: [https://aq5.epa.gov/aqsweb/airdata/download\\_files.html](https://aq5.epa.gov/aqsweb/airdata/download_files.html). The datasets are collected by the MassDEP and reported to the EPA with quality control and assurance (Ambient Air Monitoring Quality Assurance, <https://www.epa.gov/amtic/ambient-air-monitoring-quality-assurance>). Surface NO<sub>2</sub> at four sites in Eastern Massachusetts are available for 2019, including Roxbury, Von Hillern, Lynn, and Blue Hill. Data from a fifth station (at Kenmore Square) is not used in this study due to a lack of observations in 3–8 July 2019 and frequently recorded negative values. Surface O<sub>3</sub> at three stations in Eastern Massachusetts are available in 2019, including Roxbury, Lynn, and Blue Hill.

### 2.2.3. Surface and Vertical Meteorological Observations

Surface observations of hourly wind speed and wind direction are retrieved from the NOAA ISD Lite database (<ftp://ftp.ncdc.noaa.gov/pub/data/noaa/isd-lite/>). Meteorological data at three sites are used, including Logan Airport in the coastal area and Blue Hill and Hanscom Air Force Base (referred to as Hanscom later) in the inland area. Aircraft Meteorological Data Reports (AMDAR) for Logan Airport are used to evaluate modeled vertical transport qualitatively. We use hourly vertical profiles of horizontal wind at 20-m vertical resolution produced from these reports by Y. Zhang et al. (2019) and are available via <https://zenodo.org/record/3934378#.YGsWUa9Kg2z>.

### 2.2.4. Model Configuration and Experiments Design

We use the Weather Research and Forecasting with Chemistry model WRF-Chem (Fast et al., 2006; Grell et al., 2005) version 4.0 in this study. Table 1 summarizes our model configurations that are described in more detail below. Our model includes the latest iteration of the Model for Ozone and Related chemical Tracers (MOZART-T1) gas-phase chemical scheme (Emmons et al., 2020) coupled with the Georgia Institute of Technology-Goddard Global Ozone Chemistry Aerosol Radiation and Transport (GOCART) aerosol scheme. The initial and lateral chemical conditions are from the Community Atmosphere Model with chemistry (CAM-chem) (Buchholz et al., 2019) and downloaded from the NCAR Research Data Archive. Biomass burning emissions are

**Table 1**  
Key Configurations for the WRF-Chem v4.0 Simulations

Simulations	1. adjNEI11 2. wFIVE+NEI17
Anthropogenic	1. Adjusted 4 km × 4 km NEI 2011—reduced 47% mobile NO <sub>x</sub> and VOCs 2. Replaced gas emissions <sup>a</sup> in 1 with 4 km × 4 km FIVE+NEI 2017
Horizontal	D01: 3 km × 3 km over the NEUS region
Vertical	60 vertical levels from the surface to 50 hPa
Initial/boundary	Meteorology: HRRR 3 km, Chemical: CAM-Chem
Chemistry	Gas scheme: MOZART-T1, Aerosol scheme: GOCART
Other emissions	Fire: FINNv1.5, Biogenic: MEGAN
Parameterizations	Goddard, RRTMG, Thompson, revised Monin-Obukhov, Noah, YSU, G3, New TUV, Lightning-NO <sub>x</sub>
Diagnostics	Tropopause height diagnostic, tendency diagnostics for O <sub>3</sub>

<sup>a</sup>NO<sub>x</sub>, HCHO, Isoprene, C<sub>2</sub>H<sub>5</sub>OH, C<sub>2</sub>H<sub>6</sub>, CH<sub>3</sub>COCH<sub>3</sub>, CH<sub>3</sub>OH, CO, SO<sub>2</sub>, NH<sub>3</sub>, and HONO.

calculated using the Fire Inventory from NCAR (FINNv1.5) (Wiedinmyer et al., 2011). Biogenic emissions are calculated online using the Model of Emissions of Gases and Aerosols from Nature (MEGAN) module (Guenther et al., 2006). Other parameterizations include Thompson's microphysics scheme, the Rapid Radiative Transfer Model for General Circulation Models Applications (RRTMG) longwave and Goddard shortwave radiation schemes, the revised Monin-Obukhov surface layer, the Noah Land Surface Model, the Yonsei University (YSU) PBL, the New Grell cumulus scheme (G3), and the new Tropospheric Ultraviolet-Visible photolysis scheme (New-TUV). Lightning-NO<sub>x</sub> is included using the Barth et al. (2012) and Wong et al. (2013) parameterization. Tropopause diagnostic output (TROPO\_P, TROPO\_Z, TROPO\_LEV) in WRF-Chem is archived in order to compare modeled tropospheric column NO<sub>2</sub> (TCNO<sub>2</sub>) with the Pandora-derived observations. Modeled tropospheric columns are calculated by summing the partial NO<sub>2</sub> columns in each model layer from the surface to the tropopause height.

We use a single model domain (as shown in Figure S1 in Supporting Information S1), which covers the North-eastern United States (NEUS) region with constant spatial resolution at 3 km (i.e., horizontal grid spacing). The number of the model grid cells is 389 in the West-East direction and 389 in the North-South direction. The vertical coordinate comprises 60 layers below 50 hPa and 12 layers below 2 km altitude, with a center height of 28 m for the lowest layer. The simulation time ranges from 1200 UTC on 19 June 2019 to 1200 UTC on 11 July 2019, with the first 3 days used as model spin-up. The initial and lateral meteorological conditions are from the 3-km High-Resolution Rapid Refresh (HRRR) model (Benjamin et al., 2016). HRRRv3 hourly analyses data were retrieved from the HRRR archive at the University of Utah (Blaylock et al., 2017). We use nudged meteorological fields in the simulations and recycle the initial chemical fields from the previous cycle every 24-hr. We test two simulations with different high-resolution anthropogenic emissions inventories based on our/publicly available information at the time of the study to examine uncertainties in model emissions:

*Simulation adjNEI11.* The 2011 US EPA National Emission Inventory (NEI 2011v2) with 4 km resolution is regridded to the 3 km model domain. Mobile NO<sub>x</sub> and VOCs emissions (from the on-road and non-road sectors in the anthropogenic emission inventory) were reduced by 47% based on the US EPA national emissions trends from 2011 to 2019 (Air Pollutant Emissions Trends Data: National Tier 1 CAPS Trends, <https://www.epa.gov/air-emissions-inventories/air-pollutant-emissions-trends-data>). Emission trends for Massachusetts show a 44% decline over this period (Air Pollutant Emissions Trends Data: State Tier 1 CAPS Trends, <https://www.epa.gov/air-emissions-inventories/air-pollutant-emissions-trends-data>), so we do not expect our main findings would change if state-level trends were used.

*Simulation wFIVE+NEI17.* The Fuel-based Inventory of motor-Vehicle Emissions (FIVE) and NEI 2017 inventory projected for 2019 (M. Li et al., 2021; McDonald et al., 2018) is used to update trace gases emissions in the adjNEI11 simulation input, including NO<sub>x</sub>, selected VOCs species matching the MOZART-T1 mechanism (HCHO, Isoprene, C<sub>2</sub>H<sub>5</sub>OH, C<sub>2</sub>H<sub>6</sub>, CH<sub>3</sub>COCH<sub>3</sub>, and CH<sub>3</sub>OH), and other trace gases (CO, SO<sub>2</sub>, NH<sub>3</sub>, HONO). The original 4 km resolution of this inventory is regridded to our 3 km model domain. Figure S2a and Figure S2b in Supporting Information S1 compare anthropogenic NO<sub>x</sub> emissions inputs between adjNEI11 and wFIVE+NEI17 over the study region in terms of diurnal emissions and spatial distribution, respectively.

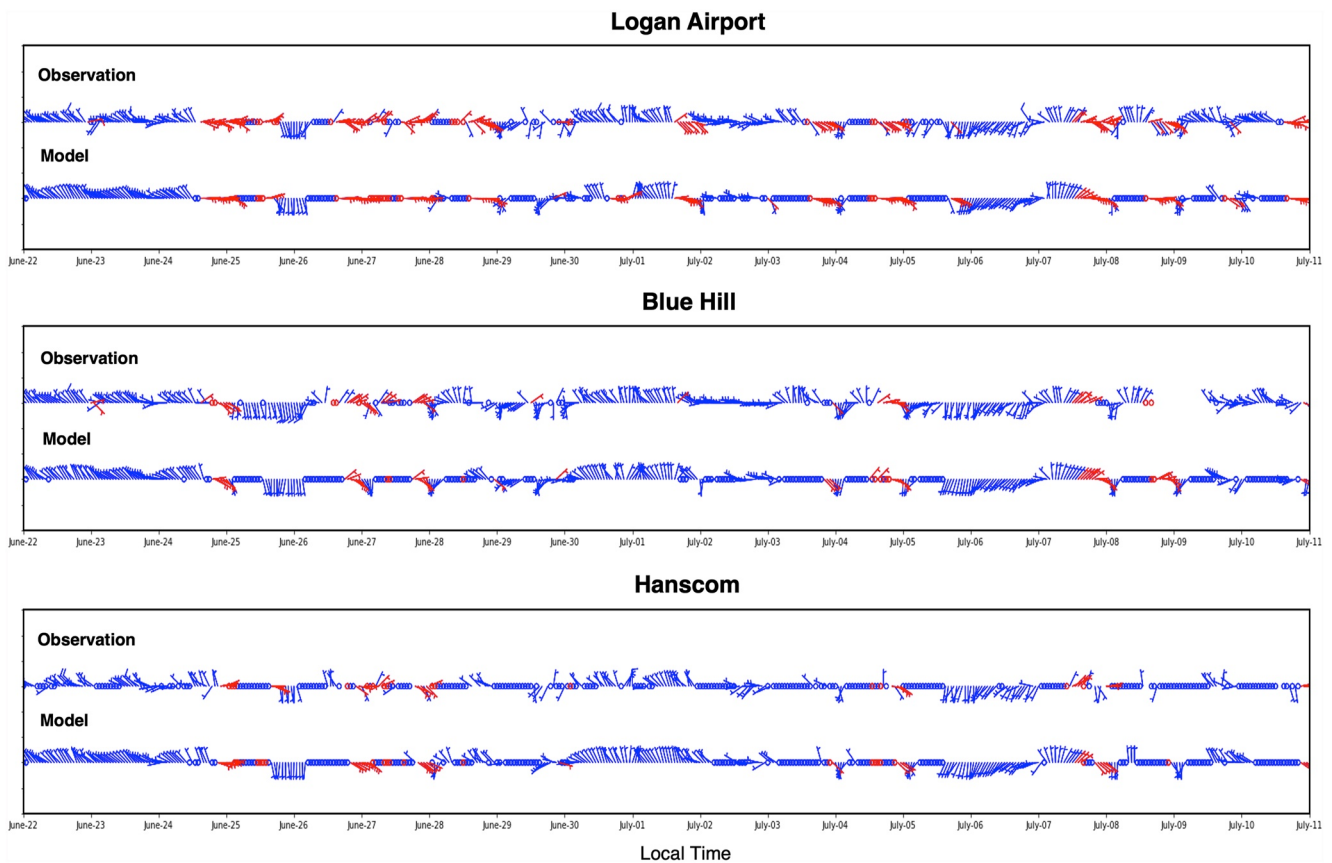


**Figure 2.** Comparison of surface wind at 10 m altitude between model results and ISD observations at Logan Airport, Blue Hill, and Hanscom sites from 2019 June 22–2019 July 10. The red arrows denote observed and modeled easterly wind ( $45\text{--}135^\circ$ ) during the sea breeze time period. Meteorological outputs between two simulations are identical as the aerosol-radiation feedback is turned off.

### 3. Results

#### 3.1. Model Evaluation

We begin with a comparison between our model simulations and available observations. Table S2 in Supporting Information S1 summarizes some statistics for model performance.

##### 3.1.1. Surface Wind Measurement

Figure 2 shows the comparison between observed and simulated surface wind vectors at Logan Airport (coastal), Blue Hill (inland), and Hanscom (inland). We first classify sea-breeze days based on the observed surface wind at Logan Airport. The red arrows in Figure 2 denote easterly wind directions between  $45$  and  $135^\circ$  (onshore winds) indicative of sea breeze activity. We acknowledge potential discrepancies in different identification methods for breeze development and therefore include a supplement analysis of air temperature and relative humidity in Figure S11 in Supporting Information S1.

A typical sea-breeze day is characterized by the onset of an easterly sea breeze at the coastal station that is sustained for a few hours duration. The onset time often shows a switch of wind direction from westerly (with northerly or southerly component) to easterly by mid-morning, with the minimum wind speed observed around 10 a.m. LT (Geddes et al., 2021). There are 10 sea-breeze days identified during the simulation time (June 24, 26–28, July 1, 3–4, 7–8, and 10). On these sea-breeze days, observed surface wind at Blue Hill and Hanscom provide an observational constraint on the extent of sea breeze inland penetration. The occurrence, inland penetration, and onset/lag time of sea breezes at these inland locations vary considerably from day-to-day, indicating diversity in sea breeze types sampled. For example, the sea breeze reached inland stations on June 24, 26–27, July 4, 7, 8, and 10. While on June 28, July 1, and 3, trivial sea breeze occurrence is recorded at the inland stations. The

various extents of inland penetration are consistent with the literature in this study region (Barbato, 1978; Geddes et al., 2021) and, as we will show, can introduce variations in the spatiotemporal distribution of air pollutants. We also note nine non-sea-breeze days dominated by other weather conditions, such as westerly prevailing winds, or thunderstorms and fronts.

The model generally reproduced sea-breeze winds at both the coastal and inland sites. Where possible, we evaluated: the occurrence of a sea breeze; onset time; duration; and extent of inland penetration. First, we find the model captured all observed sea-breeze days in terms of their occurrence and inland penetration. However, the model also predicts sea breeze events on June 30 and July 5 which have been classified as non-sea breeze days based on the observations at Logan. This could highlight a potential difficulty in classifying conditions based on a limited set of meteorological observations. We also find that accurate modeling of onset time and duration of a sea breeze in each case remains a challenge, at least partly, associated with the model uncertainties in PBL schemes or air-sea interactions along the coastal regions. Biases in wind speed and direction on a particular day can substantially affect the accuracy of modeled NO<sub>2</sub> and O<sub>3</sub> concentrations. For example, a wind direction bias during rapid changes of wind direction and a slightly underestimated minimum speed may contribute to a high pollution biases (e.g., June 26 and 27). Still, the model performs well overall in reproducing the surface transport in sea breeze events.

Figure S3 in Supporting Information S1 shows the comparison of modeled vertical profiles of horizontal winds with AMDAR observation over Logan Airport. We find that sea-breeze circulations often develop within a very shallow layer in the boundary layer. The low-level sea breeze circulation, indicated by the red arrows in AMDAR wind profiles, have a depth below 0.5 km on most sea breeze days (and a depth of ~1 km in three cases, July 4, 7, and 8). The figure shows that our simulation successfully captures these vertical characteristics of the occurrence and depth of sea breeze circulations. Our observed results are consistent with the findings from Barbato (1978), who showed that the vertical extent of the sea breeze inflow varies between 330 and 1,230 m, which is within the normal range for a sea breeze in the middle latitudes. From a climatological perspective, Geddes et al. (2021) indicate that the average height of the sea breeze system in 2010–2019 is on the order of 300 m. They observed a very stable atmosphere near the surface, more consistent with marine atmospheric conditions, with neutral to unstable conditions immediately aloft, which provides relevant insights for us to understand our observed vertical structure in the individual cases. Further, we add a caveat that our selection of the 10 sea breeze cases during the specific summer of 2019 may not necessarily represent the climatological behavior of sea breeze properties in this urban area.

### 3.1.2. Surface NO<sub>2</sub> Measurement

Figure 3 shows the time series of surface NO<sub>2</sub> measured at the four sites in our study domain compared with the modeled surface NO<sub>2</sub> from the collocated model grid cell (i.e., point-to-point comparison using the nearest model grid cell to the station). We evaluate the output from simulations with two different anthropogenic emission inputs: adjNEI11 and wFIVE+NEI17 (described above). This evaluation aims to answer: (a) Can we determine which simulation better represents the primary NO<sub>x</sub> emissions' magnitude and spatiotemporal variability in this region? and (b) How does the model accuracy vary between sea-breeze and non-sea-breeze days?

We find that the choice of anthropogenic NO<sub>x</sub> inventory plays an important role in the performance of surface NO<sub>2</sub> magnitude in the Greater Boston region. Although both simulations resolved urban-suburban differences well, the adjNEI11 simulation overestimated surface NO<sub>2</sub> significantly (RMSE<sub>adjNEI11</sub> = 8.79, NMB<sub>adjNEI11</sub> = 0.62). This indicates that reducing the mobile (on-road and off-road) NO<sub>x</sub> emissions from NEI2011 inventory by half (according to the trend in NEI from 2011 to 2019) is insufficient to accurately represent local emissions in 2019. The wFIVE+NEI17 simulation performs better in surface NO<sub>2</sub> (RMSE<sub>wFIVE+NEI17</sub> = 5.91, NMB<sub>wFIVE+NEI17</sub> = 0.23), especially at the urban sites, suggesting a better representation of local anthropogenic NO<sub>x</sub> emissions for 2019.

The temporal dynamics of emissions are not captured perfectly by either inventory, as indicated by a moderate hourly correlation across all sites (R<sub>wFIVE+NEI17</sub> = 0.63, R<sub>adjNEI11</sub> = 0.68). We examine the model diurnal performance by different sites and weather scenarios to understand the discrepancies in more detail (Table S2 in Supporting Information S1). The correlation coefficient statistics indicate that: (a) Both simulations have a moderate correlation with the hourly NO<sub>2</sub> observed at most individual sites, except for a weak correlation with the Lynn site. This is likely due to transport errors at this near-coast suburban region, since both simulations show a mismatch with the observed rapid increases of surface NO<sub>2</sub> at Lynn on individual days (e.g., June 26 and 27);

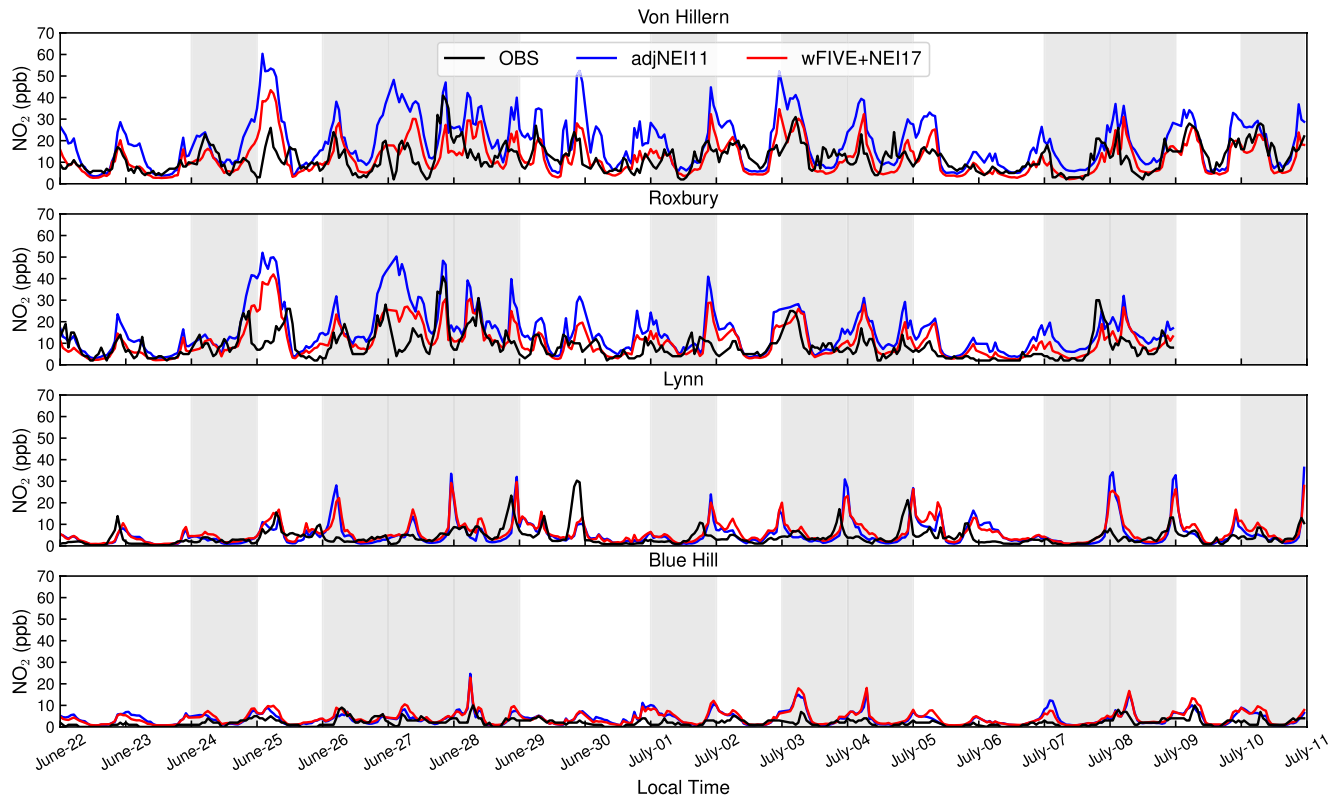


**Figure 3.** Comparison of surface  $\text{NO}_2$  between WRF-Chem simulations and surface observation from 2019 June 22–2019 July 10 at 4 sites. The shading denotes 10 sea breeze days classified by inspection of the wind observations at Logan, where the onset time of sea breezes is mostly between 9 a.m. LT to 12 p.m. LT.

(b) The diurnal performance varies with weather scenarios and days. For example, westerly prevailing days have the best diurnal performance over other scenarios, with a strong overall correlation with observed hourly  $\text{NO}_2$  (e.g.,  $R_{wFIVE+NEI17} = 0.75$ , daily range in  $[0.42, 0.90]$ ). In contrast, sea-breeze days have an overall moderate correlation and a broader range of daily diurnal correlation (e.g.,  $R_{wFIVE+NEI17} = 0.62$ , daily range in  $[-0.23, 0.86]$ ), likely associated with the uncertainty in modeling the onset time of sea breeze and wind. This implies that the challenges during sea-breeze conditions may degrade the overall model performance in coastal regions. The thunderstorm or front scenario is another complex weather condition with relatively weak performance compared to westerly prevailing days. Although we do not focus on these days for our analysis, we briefly address the possible reasons together with the  $\text{O}_3$  evaluation later.

Overall, the comparison indicates that our model performs reasonably at reproducing surface  $\text{NO}_2$  patterns in the region, even during sea breezes, and the wFIVE+NEI17 (projected to 2019) inventory seems to represent more realistic  $\text{NO}_x$  emissions during our study period.

### 3.1.3. Pandora Column $\text{NO}_2$ Measurement

Surface  $\text{NO}_2$  alone may be insufficient to represent the primary  $\text{NO}_x$  emission and its diurnal behavior, partly due to the impact of PBL evolution throughout the day. Therefore, we further apply Pandora tropospheric  $\text{NO}_2$  observations at BU to provide an additional evaluation of the emissions used in our model scenarios. Figure 4 shows the tropospheric  $\text{NO}_2$  column comparison between the Pandora observations at BU, and collocated output from the two simulations.

Both simulations are able to reproduce the general temporal variability observed in tropospheric  $\text{NO}_2$ . Quantitatively, the simulations captured the daily variability of column  $\text{NO}_2$  with strong correlation ( $R_{wFIVE+NEI17} = 0.85$  for daily 2 p.m. comparison;  $R_{wFIVE+NEI17} = 0.78$  for daily 6 p.m. comparison) and hourly variations of column  $\text{NO}_2$  with moderate correlation ( $R_{wFIVE+NEI17} = 0.64$ ,  $R_{adjNEI11} = 0.60$ ). Compared to the daily variation, the relatively weaker performance in diurnal variation of tropospheric column  $\text{NO}_2$  is again likely associated with small errors in modeling the onset time of sea breeze that become very important due to rapid changes in  $\text{NO}_2$  column



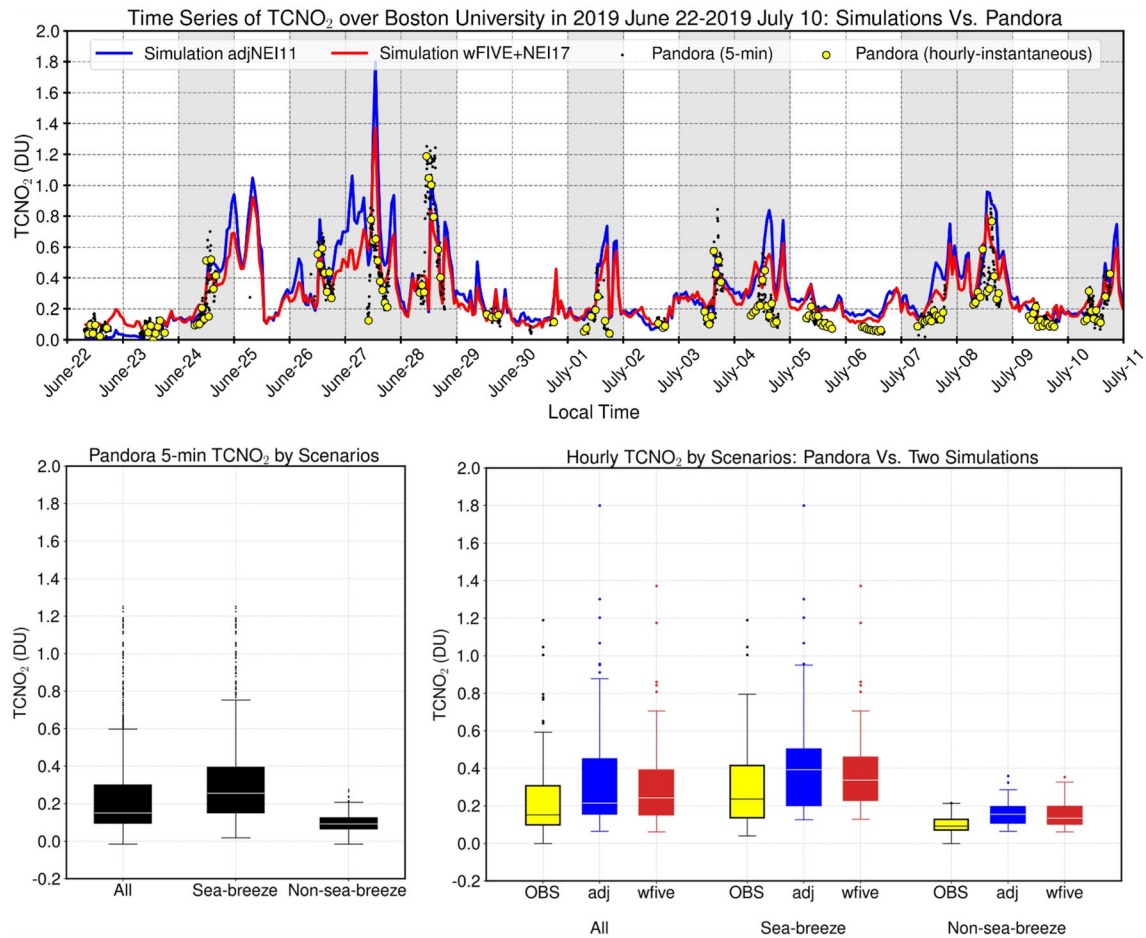


**Figure 4.** (upper) Comparison of tropospheric column  $\text{NO}_2$  ( $\text{TCNO}_2$ ) between WRF-Chem simulations and Pandora observation at Boston University from June 22 to 10 July 2019. The black dots and yellow circles denote 5-min and hourly-instantaneous (i.e., the 5-min average value occurring on the hour (e.g., value at 2:00 p.m., at 3:00 p.m., etc.)) Pandora data, respectively. The blue and red lines represent simulation adjNEI11 and wFIVE+NEI17, respectively. The shading denotes 10 sea breeze days classified by inspection of the wind observations at Logan. (Bottom left) BU Pandora 5-min  $\text{TCNO}_2$  box and whisker plots grouped by 19 all days, 10 sea-breeze days, and 9 non-sea-breeze days. (Bottom right) Hourly  $\text{TCNO}_2$  comparison between BU Pandora hourly-instantaneous data (labeled as “OBS”) and two simulations adjNEI11 (labeled as “adj”) and wFIVE+NEI17 (labeled as “wfive”).

abundance. This is supported by the scatter plot in Figure S4 in Supporting Information S1, which shows a relatively tight distribution at low column abundances, but a larger spread in the distribution at higher column abundances (which tends to be observed primarily during sea-breeze days, Figure 4). Therefore, a mismatch of the timing in peak  $\text{NO}_2$  between modeled and observed tropospheric column  $\text{NO}_2$  weakens the hourly correlation.

Generally, we find a clear response in the tropospheric column  $\text{NO}_2$  to the sea-breeze days. Both Pandora observations and model results show a rapid increase of  $\text{NO}_2$  column densities during sea-breeze days in the Boston area. This provides further evidence of an accumulation of primary emissions in the upper air over the urban Boston region, as pointed out in Geddes et al. (2021) using a climatological analysis of available surface  $\text{NO}_2$  monitoring. We group the timeseries by sea-breeze and non-sea-breeze cases to better illustrate this sea-breeze role on  $\text{TCNO}_2$  magnitude and corresponding model performance. We note how the 5-min Pandora observations resolve rapid fluctuations on sea-breeze days, revealing that the sea breeze can impact tropospheric  $\text{NO}_2$  on the timescale of minutes. This distinct and rapid diurnal variation of tropospheric column  $\text{NO}_2$  is not resolved by hourly instantaneous model output (nor hourly average monitoring data). Therefore, we show 5-min Pandora data first, and then make a fair “apples to apples” evaluation by sampling the 5-min Pandora data at hourly intervals for comparison with the hourly model output.

The boxplot of 5-min Pandora observations shows that the sea-breeze scenario dominates the high  $\text{TCNO}_2$  observed in this region. Later, we use the third quartile of observed  $\text{TCNO}_2$  ( $Q_3 = 0.4$  DU) as an indicator for

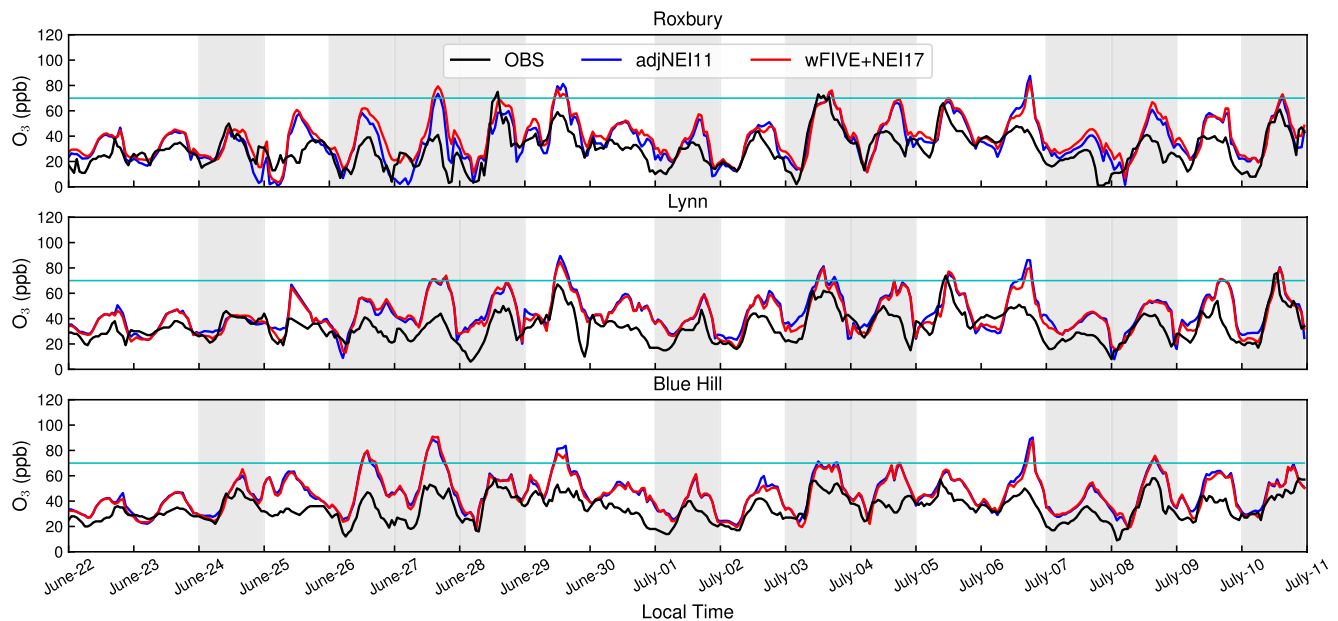


**Figure 5.** Comparison of surface  $O_3$  between WRF-Chem simulations and surface observation from 2019 June 22–2019 July 10 at 3 sites. The shading denotes 10 sea breeze days classified by inspection of the wind observations at Logan. The aqua line marks  $O_3$  concentrations of 70 ppb.

high  $TCNO_2$  “hot spots”. We compare the modeled  $TCNO_2$  with hourly averaged Pandora  $TCNO_2$  in the boxplots of Figure 4. Both simulations are able to capture the coincidence of high  $NO_2$  on sea breeze days compared to other conditions, but the wFIVE+NEI17 scenario performs better in representing the absolute values, especially the highest  $TCNO_2$  (e.g., in terms of third quartile and outliers).

Considering the model performance for surface  $NO_2$  and  $TCNO_2$  together, we infer that the wFIVE+NEI17 inventory is a more accurate representation of the 2019  $NO_x$  emissions over the urban core. The overestimate of  $NO_x$  emissions in the scaled NEI2011 inventory is consistent with the evidence of uncertainties in mobile emissions estimated by the NEI (Anderson et al., 2014; McDonald et al., 2018; Souri et al., 2016; Travis et al., 2016), and this work may add to this evidence. We note that the weekday-weekend emissions difference is reflected in wFIVE+NEI17 but not in adjNEI11, and the diurnal trend of wFIVE+NEI17  $NO_x$  emission has an earlier increase on weekdays than on weekends. The discrepancies between the two inventories are particularly high in suburban areas of our study region (see Region two in Figure S2a in Supporting Information S1). We also note that M. Li et al. (2021) find the updated FIVE18 (FIVE inventory updated for 2018) is in good agreement with NEI17 over the Continental United States, in contrast to discrepancies reported between FIVE and the NEI for previous years. More Pandoras and surface constraints in future work may help interpret the performance of these emission inventories over our study region.

### 3.1.4. Surface $O_3$ Measurement

Figure 5 shows the comparison of surface  $O_3$  between simulations and observations at urban (Roxbury) and suburban (Lynn and Blue Hill) sites. With this evaluation we aim to answer: (a) Can we determine which simulation better represents the secondary  $O_3$  pollutant’s magnitude and spatiotemporal variability in the region? (b) How does the model accuracy vary between sea-breeze and non-sea-breeze days?

The comparison shows that model performance in representing the magnitude and diurnal variations of surface  $O_3$  is similar in either simulation. Both have a strong correlation with observed hourly  $O_3$  variations ( $R_{wFIVE+NEI17} = 0.71$ ,  $R_{adjNEI11} = 0.72$ ). We note that the model successfully reproduces nighttime  $O_3$ , especially at the urban site (Roxbury), which indicates an accurate representation of  $O_3$  titration from local  $NO_x$  emissions. The wFIVE+NEI17 simulation performs better overall in reproducing nighttime  $O_3$  (e.g., June 24, June 26), which provides additional evidence that the  $NO_x$  emissions from this scenario are more appropriate. However, there is a tendency to overestimate daily peak  $O_3$  on individual days, leading to an overall overestimate of  $O_3$  in both simulations ( $RMSE_{wFIVE+NEI17} = 14.95$ ,  $NMB_{wFIVE+NEI17} = 0.32$ ,  $RMSE_{adjNEI11} = 14.76$ ,  $NMB_{adjNEI11} = 0.30$ ).

This implies that factors in addition to overestimating local  $\text{NO}_x$  sources play a predominant role in the modeled ozone bias in this region.

We find that modeled  $\text{O}_3$  performance varies with atmospheric conditions. Westerly prevailing days show the best performance, with moderate to strong correlation for individual days (e.g.,  $R_{wFIVE+NEI17} = 0.73$ , daily range in [0.52, 0.92]). In contrast, days with precipitation (June 25, 29–30, July 6) show a large  $\text{O}_3$  bias in magnitude and diurnal variations. Both surface  $\text{NO}_2$  and  $\text{O}_3$  have weak model performance on these rainy days (June 25, 29–30, July 6), which could be evidence of underestimated precipitation and wet scavenging on trace gases (J. Li et al., 2021) and an indication of model uncertainties in photochemistry related to mispredicted clouds development. Accurate precipitation simulation requires sufficient observation data and sophisticated assimilation methods to improve the uncertainties on model spin-up and rapid error growth problems (Akbari Asanjan et al., 2018), but these conditions are not the focus of this manuscript and could be the subject of future modeling investigations.

Modeled  $\text{O}_3$  performance varies from day-to-day in the sea-breeze scenarios. For example, June 24, June 28, July 3, and July 10 show relatively accurate ozone simulation, while June 26–27 show a larger bias. Quantitatively, modeled magnitude and diurnal correlation show a broad range in sea-breeze days (e.g.,  $R_{wFIVE+NEI17} = 0.72$ , daily range in [0.15, 0.92]). We use a process analysis in Section 3.2.3 to explore the various drivers of model  $\text{O}_3$  performance on specific sea breeze days.

### 3.2. Sea Breeze Impacts on Spatiotemporal Distribution of $\text{O}_3$ and $\text{NO}_2$

Leveraging our model run that includes many examples of sea breezes, we investigate the general impact of sea breezes on the predicted spatiotemporal variability of primary emissions and secondary  $\text{O}_3$  pollution. The 3-km resolution model output allows us to determine the diurnal and daily changes in the spatial distribution of pollutants on sea-breeze days, and identify “hot spots” that may indicate gaps in current monitoring and opportunities for additional ground-based and remote sensing measurements. Based on our evaluation above, we focus on output using the wFIVE+NEI17 (projected to 2019) inventory simulation. We begin by focusing on the role of sea breeze events on modeled surface concentrations of  $\text{NO}_2$  and  $\text{O}_3$  with implications for surface monitoring capabilities. We then discuss the importance of sea breezes on tropospheric  $\text{NO}_2$  columns, which has relevance in particular for remote sensing applications.

#### 3.2.1. Daily and Diurnal Variability of Surface $\text{O}_3$ and $\text{NO}_2$

Figure 6 shows modeled surface  $\text{O}_3$  (with contours of modeled surface  $\text{NO}_2$ ) and surface wind vector distribution at 2 p.m. and 6 p.m. on selected sea-breeze days and non-sea-breeze days that showed good agreement with the available observations (plots for all cases are shown in Figure S5 in Supporting Information S1). 2 and 6 p.m. are selected due to being within obvious sea breeze impact hours and close to overpass times of remote sensing observations (either afternoon-overpasses from polar-orbit or late day observations from geostationary orbit). Compared with the non-sea-breeze cases, the distinctive feature on the sea-breeze days is a convergence zone of elevated  $\text{O}_3$  characterized by a steep  $\text{O}_3$  gradient over land. The formation of this steep  $\text{O}_3$  gradient is consistent with previous model findings from the Chesapeake Bay area (Loughner et al., 2014). This convergence zone over the urban region causes high air-pollution concentrations on both sides of the breeze front to converge while bringing cleaner air from the marine and rural/suburban areas to the convergence zone.

On days that develop sea breeze cases, we find that mornings (10 a.m. LT, see Figure S5 in Supporting Information S1) are often characterized by accumulated local  $\text{NO}_x$  emissions (steep  $\text{NO}_2$  gradients and the maximum  $\text{NO}_2 > 10$  ppb) due to calm wind fields overland, and see a concomitant  $\text{NO}_x$  titration effect on  $\text{O}_3$  concentrations in the urban core. Exceptions occur on June 24, July 1, and July 7 which each starts with a stronger wind field overland (in the overall domain on July 1 and 7, or in a limited urban area on June 24). By 2 p.m. LT (Figure 6 and S5 in Supporting Information S1), easterly sea breezes have penetrated inland, reaching varying extents along the coastline depending on the case. At this time, the full inland penetration of the sea breeze front reaches up to ~20 km away from the coastal Logan Airport location. The convergence zone of steep  $\text{O}_3$  gradient appears in the vicinity of the breeze front. Modeled surface  $\text{O}_3$  concentrations become particularly elevated (>70 ppb) on June 26–28, July 3–4, July 8 and 10. Among these days, elevated  $\text{O}_3$  is also recorded by at least one of the monitoring stations on June 28, July 3, and July 10. Both observations and model results show that the sea breeze days that start with weaker winds over land (which less effectively ventilate local emissions) can result in elevated

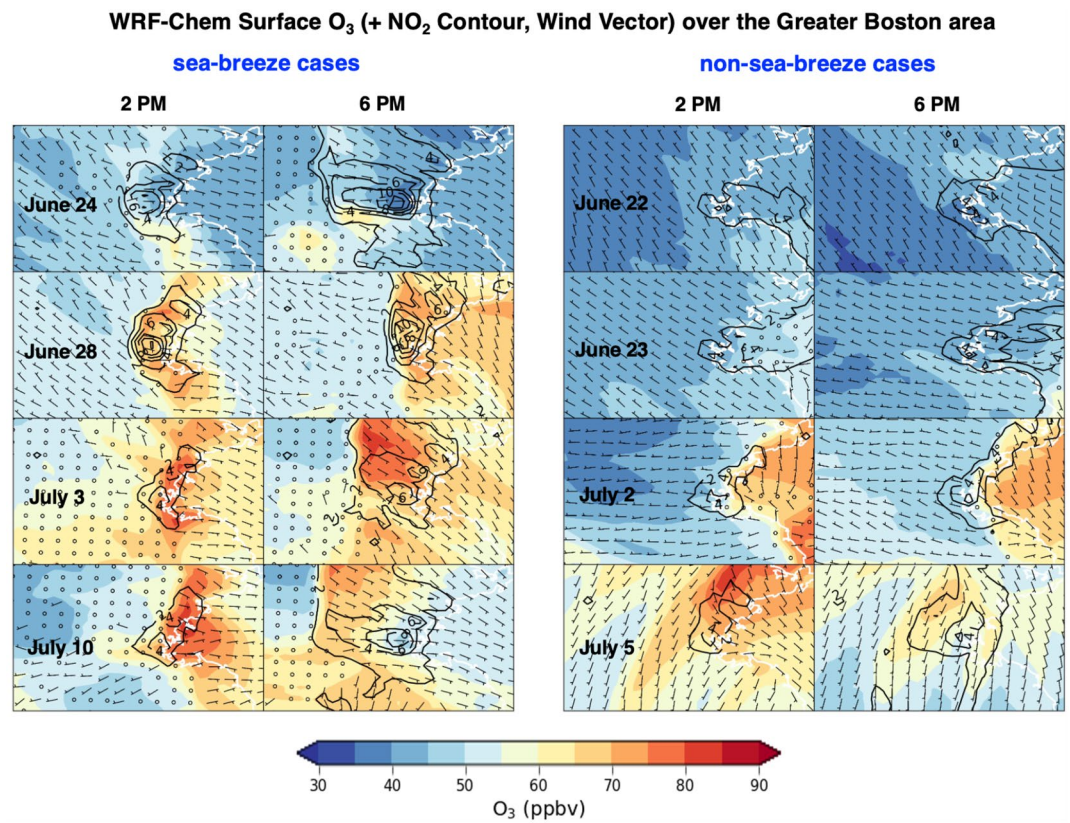


**Figure 6.** Modeled surface O<sub>3</sub>, NO<sub>2</sub> contour (black lines), and wind vector (black arrows) distribution at 2 and 6 p.m. LT on sea-breeze days and non-sea-breeze days. Plots for all cases at 10 a.m., 2 p.m., and 6 p.m. LT are shown in Figure S5 in Supporting Information S1. The coastline is shown in white. The density of wind barbs was reduced by half along the longitude and the latitude for visualization.

O<sub>3</sub> concentrations, suggesting that the accumulation of local primary pollutants due to the weak ventilation and subsequent local production of O<sub>3</sub> is an important driver on the worst O<sub>3</sub> sea breeze days (as opposed to being impacted by precursors transported from upwind regions).

By the later afternoon (at 6 p.m. LT), O<sub>3</sub>-rich air further penetrates inland and maintains elevated concentrations. The penetration of the O<sub>3</sub>-rich air exhibits large spatial variability from day-to-day, with an inland penetration from less than 20 km to 50–60 km away from the coastline. The variable inland penetration distance coincides with varying penetration wind speeds from day-to-day. Of the simulated cases, inland penetration wind speeds ranged from a maximum of ~8 km/hr (e.g., June 26 in Figure S5 in Supporting Information S1) to a minimum speed of near zero (e.g., stagnant air on June 28).

### 3.2.2. Surface O<sub>3</sub> and O<sub>x</sub> Hotspots

Figure 7 shows a map of counted hours when modeled surface O<sub>3</sub> exceeded 70 ppb, along with the locations of current O<sub>3</sub> ground-based monitoring. We find major hot spots of O<sub>3</sub> pollution (hourly O<sub>3</sub> > 70 ppb) inland, along the coast, and in overseas regions. This pollution heterogeneity overland is dominated by sea-breeze days, where we find areas of high O<sub>3</sub> over some inland suburbs and suppressed O<sub>3</sub> concentrations in the immediate urban core. Non-sea-breeze days have a more uniform distribution of O<sub>3</sub> pollution overland (from low upwind to higher downwind) due to more synoptic advection patterns. These days see higher O<sub>3</sub> concentrations mainly overseas, downwind of the urban emissions.

We additionally calculate “O<sub>x</sub>” hot spots to help interpret the heterogeneity in O<sub>3</sub> pollution (Figure 7, right). Defining O<sub>x</sub> as NO<sub>2</sub> + O<sub>3</sub> helps attribute the spatial patterns between near-field titration of O<sub>3</sub> by high NO sources from chemical O<sub>3</sub> production and transport (assuming negligible impacts of direct NO<sub>2</sub> emissions). The spatial distribution of high O<sub>x</sub> hours in the sea-breeze scenario is consistent with our observational analysis in Geddes

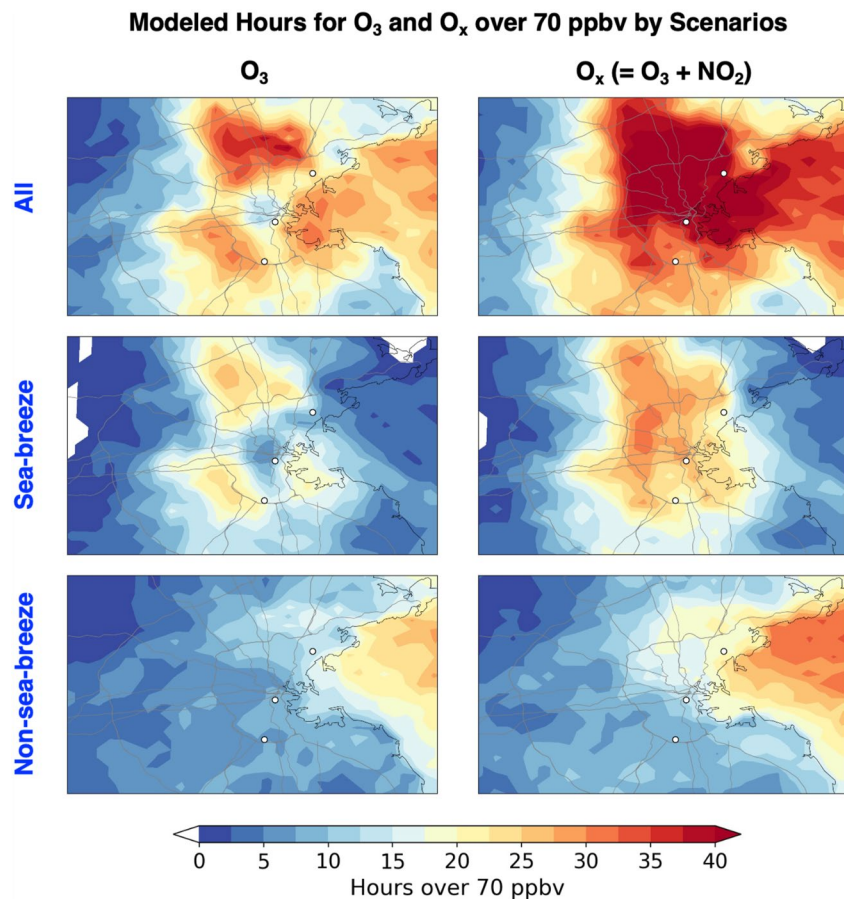


**Figure 7.** Modeled hours for O<sub>3</sub> (left) and O<sub>x</sub> (right) over 70 ppbv for 19 all days, 10 sea-breeze days, and 9 non-sea-breeze days. The white circle denotes the three surface O<sub>3</sub> monitoring sites used in this study.

et al. (2021), where we inferred the presence of large horizontal gradients of secondary air pollution across monitoring stations during sea breezes. Even after accounting for near-field titration by NO, the model predicts sharp gradients over relatively small distances within the urban region. Moreover, the model predicts an enhancement of secondary air pollution on sea breeze days further inland, over regions that are not currently covered by routine monitoring sites for O<sub>3</sub> and NO<sub>2</sub>. As shown in the diurnal distributions, the various extent of sea-breeze inland penetration can bring O<sub>3</sub>-rich air to the far inland area. The increase of O<sub>x</sub> inland indicates that secondary O<sub>3</sub> production takes place while the breeze penetrates inland, impacting the O<sub>3</sub> distribution. Notably, by comparing O<sub>x</sub> with O<sub>3</sub> hot spots, we find that the sea breeze days specifically result in suppressed O<sub>3</sub> pollution within the urban core due to the titration by NO sources that are accumulated locally. On non-sea breeze westerly days, these emissions are more efficiently ventilated.

Together, the interactions between O<sub>3</sub> photochemistry, sea breeze inland penetration, and NO<sub>x</sub> titration effects contribute to the O<sub>3</sub> pollution heterogeneity overland that is poorly represented by the current routine observations. While conventional wisdom in the Greater Boston region is that poor air quality can be largely attributed to non-local precursors being transported from the southwest direction (due to the predominance of westerly conditions in the Northeast U.S. region), our modeling suggests that the additional importance of sea breezes on deteriorating local air quality could be underestimated simply due to current monitor placement. We explore this in more detail below using process-level diagnostics from the model in Section 3.2.3.

Our analysis of O<sub>3</sub> hot spots brings up an important question relevant to the air quality community: What typical conditions favor O<sub>3</sub> pollution in the Greater Boston area? Based on the observations and model results, two typical conditions favor high hourly ozone over 70 ppb (8-Hour ozone over 70 ppb is defined as an ozone exceedance day in EPA standard). One is characterized by southwesterly winds on non-sea-breeze days, and the

associated non-local pollution sources. This is supported by the Massachusetts 2019 Air Quality Report (Massachusetts 2019 Air Quality Report, 2020) saying that  $O_3$  exceedances typically occur in Massachusetts when a high pressure south of New England creates a broad and slow southwesterly airflow containing precursors from the upwind coastal urban corridor to New England. It is fair to say that the current surface monitoring network covers important upwind-downwind transect under southwesterly flow (e.g., Blue Hill, Roxbury, Lynn) and may provide sufficient monitoring of pollution when these conditions prevail.

Here, we identify the additional importance of sea breezes. Not all sea-breeze days directly lead to elevated  $O_3$  pollution levels, but Geddes et al. (2021) showed using limited observations that  $O_3$  can achieve comparable midday concentrations as those on westerly-prevailing conditions (with sea breeze days more impacted by local production due to calm morning conditions, and a smaller background input from upwind). Our model results further confirm this, and provide a full picture of the spatiotemporal distribution. We find that  $O_3$  pollution on sea breeze days is unevenly distributed in space, and poorly represented by the current monitoring network. Future field experiments or even additional routine monitoring observations, particularly filling in the monitoring gap in some inland suburbs, would improve our understanding of the importance of the sea breeze on air quality and help monitor changes over the next few decades.

### 3.2.3. Diagnosing Processes Contributing to the $O_3$ Pollution in Sea Breezes

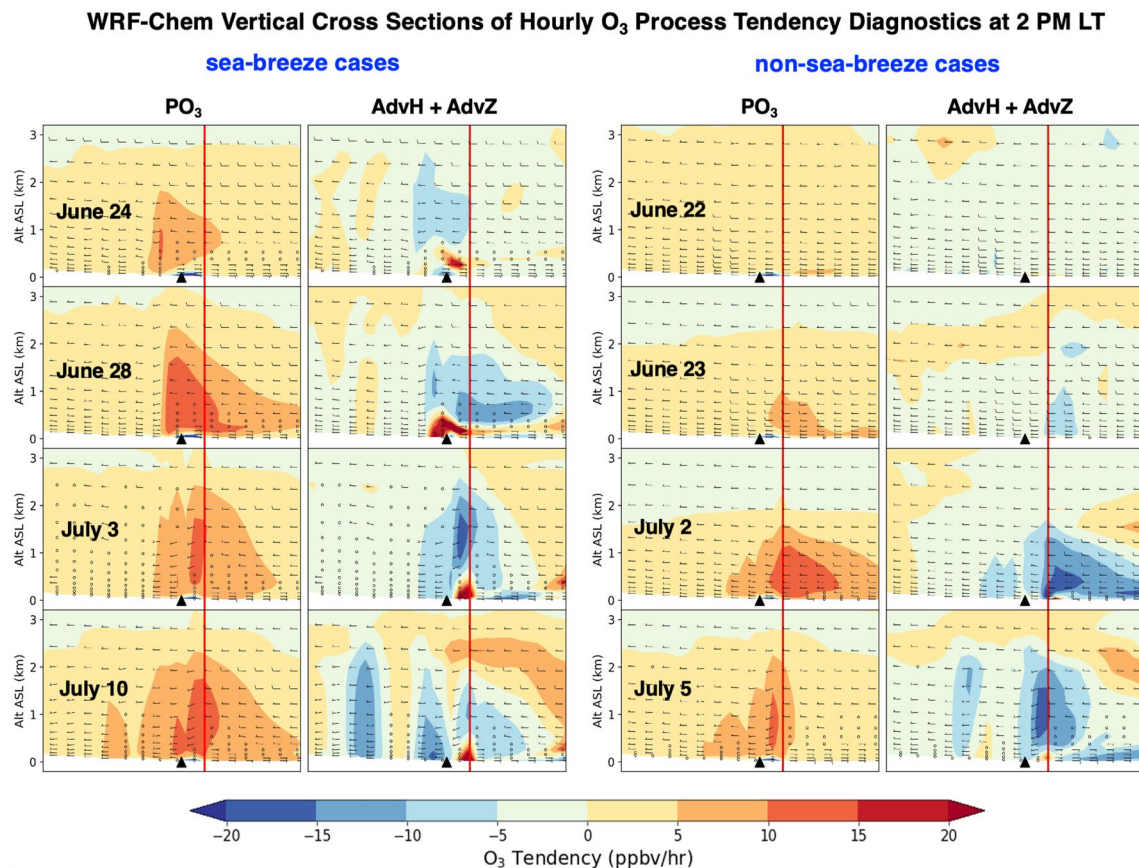
Chemical transport models offer the unique opportunity to diagnose specific processes (relating to atmospheric dynamics and chemical production) that govern the occurrence of high  $O_3$  during sea breeze events. Here, we apply WRF-Chem process diagnostic tools to quantify the contribution of these processes to high  $O_3$  pollution and interpret the interactions between dynamical and chemical processes affected by the sea breeze system.

Figure 8 shows longitude-altitude curtain plots along 42.35 N latitude (line shown in Figure 1) of WRF-Chem  $O_3$  tendencies, including net chemical  $O_3$  production ( $PO_3$ ) and the sum of horizontal and vertical advection of  $O_3$  ( $AdvH + AdvZ$ ), at 2:00–3:00 p.m. LT (18:00–19:00 UTC) on the same days as shown in Figure 6. Sea breeze days with elevated  $O_3$  (e.g., June 28, July 3, and July 10) show efficient photochemical production ( $PO_3 > 10$  ppb/hr) in the upper boundary layer (up to 1–2 km) over the urban region and rapid convergence over land ( $O_3$  advection  $> 20$  ppb/hr) near the surface (up to 300–500 m) due to the impact of sea breeze circulation. Rapid  $O_3$  convergence (positive advection tendency) within the convergence zone and considerable divergence (negative advection tendency) outside of it dominate the formation of the steep  $O_3$  gradients near the surface. During sea breeze development, inland penetration of the convergence zone (see July 3 hourly diagnostics as an example in Figure S6 in Supporting Information S1) results in elevated  $O_3$  ( $> 70$  ppb) at individual sites. In contrast, the sea-breeze case with lower  $O_3$  level (e.g., June 24) shows insufficient photochemical  $O_3$  production over the urban region and less  $O_3$  convergence impact on the surface over land.

Westerly days with low  $O_3$  levels over land may have strong photochemical  $O_3$  production, but this production occurs offshore (e.g., July 2). Southwesterly days with elevated  $O_3$  levels (e.g., July 5) do not show the same small-scale features observed on sea-breeze days, consistent with the role of synoptic-scale systems on non-local source transport.

### 3.2.4. Variability in Tropospheric $NO_2$

We next examine the relevance of our modeling to observations of tropospheric  $NO_2$  columns that would be derived from the ground- or satellite-based remote sensing. Figure 9 shows the modeled tropospheric  $NO_2$  column distribution at 2 and 6 p.m. for our simulated sea-breeze and non-sea breeze days. The tropospheric  $NO_2$  column on non-sea-breeze days, especially the westerly prevailing days, has a clear signal of local  $NO_x$  emissions being ventilated and transported over the sea. This implies that it has a lower accumulation of  $NO_x$  emissions due to the mixing or dilution. In contrast, sea breeze days have steep gradients of tropospheric  $NO_2$  column over land, ranging from almost no pollution to the highest nearby the sea breeze front. These model results suggest that sea-breeze development profoundly influences the diurnal tropospheric  $NO_2$  pattern and spatial gradient over the Greater Boston region, and can drive rapid spatiotemporal changes in column abundance. While mornings begin with weak offshore winds, the onset of sea breeze around 10 a.m. LT gradually reshapes the air mass of local anthropogenic  $NO_x$  emissions from the east to the western boundary. By 2 p.m. LT (Figure 9), the steep gradient of tropospheric  $NO_2$  just inland of the coast reflects the location of the sea-breeze front. By later afternoon (6 p.m. LT), inland penetration of the breeze can lead to a westward spreading of urban emissions into the suburban areas, still with a sharp inland boundary and steep gradient of tropospheric  $NO_2$ . Daily variability in the onset



**Figure 8.** WRF-Chem O<sub>3</sub> process diagnostics for net chemical O<sub>3</sub> production (PO<sub>3</sub>) and the sum of horizontal and vertical ozone transport (AdvH + AdvZ) at 2 p.m. LT on sea-breeze days (left) and non-sea-breeze days (right), respectively. The red line denotes the location at Logan Airport, as a rough boundary between inland and sea areas. The black triangle denotes the location at BU.

time of sea breeze and inland penetration length would drive variability in these inland suburbs, posing challenges to ground-based sea-breeze monitoring. This inland advancement of the high NO<sub>2</sub> plume later in the afternoon would not have been previously observed by current low earth orbit satellite instruments (which overpass either in the morning or early afternoon), but could be captured by forthcoming geostationary measurements.

To emphasize the importance of sea breeze days on elevated NO<sub>2</sub> columns, Figure S8 in Supporting Information S1 shows a map of counted hours in simulated tropospheric NO<sub>2</sub> column over 0.4 DU for all days, then separated by sea-breeze days and non-sea-breeze days respectively. Major hot spots of tropospheric NO<sub>2</sub> are located in the urban core over the Greater Boston area, nearby the local NO<sub>x</sub> emission sources. Sea-breeze days dominate the high tropospheric NO<sub>2</sub> hours, which are rarely observed during predominantly westerly conditions. The predicted accumulation of NO<sub>2</sub> column abundance locally during sea breeze days is consistent with preliminary findings from TROPOMI satellite observations shown in Geddes et al. (2021). Spatially allocating other Pandoras across the urban area could be of great importance for monitoring and evaluation of satellite-based tropospheric NO<sub>2</sub>. Based on the simulated distribution of NO<sub>2</sub> hot spots, the BU Pandora does tend to capture the temporal and spatial peak pollution of sea breezes (occurring ~2 p.m. LT at this location). The elevated NO<sub>2</sub> pollution during sea-breeze cases highlights the importance of sea-breeze monitoring and improving remote sensing retrievals under these conditions.

The considerable hours of high tropospheric NO<sub>2</sub> outside the urban core (Figure S8 in Supporting Information S1) indicate dynamic impacts on redistributing the local NO<sub>x</sub> emissions to both inland suburban and over-sea regions. This is particularly true when looking at the diurnal patterns on sea breeze days, where the TCNO<sub>2</sub> hot spots gradually switched from coastal offshore areas in the morning to inland areas in the afternoon. Allocation of Pandoras in the inland suburban regions could support and benefit geostationary satellite retrieval evaluation

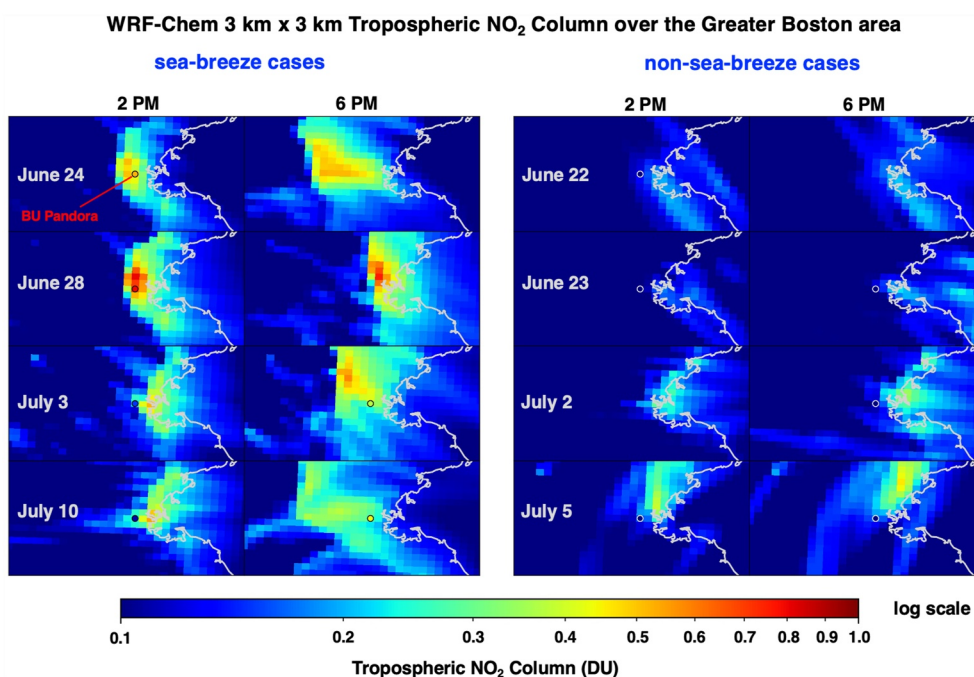


**Figure 9.** Modeled tropospheric NO<sub>2</sub> column distribution at 2 and 6 p.m. LT in sea-breeze days (left) and non-sea-breeze days (right). Available instant Pandora data is overplotted. Plots for all cases are in Figure S7 in Supporting Information S1.

during sea breezes. As of the end of 2021, additional Pandora measurements have become available in the Greater Boston region (at Harvard, Blue Hill, and Lynn, in addition to BU) to increase the coincident spatial coverage. Still, we find that to meet the challenge of geostationary satellite monitoring on sea breeze impacts, it would be helpful to allocate Pandoras at more suburban/inland sites (e.g., west of the urban region, Hanscom) and coastal sites (e.g., Logan Airport, Harbor Island). Co-allocation of Pandoras with wind monitoring sites (e.g., Logan Airport, Blue Hill, Hanscom) is especially helpful for sea breeze studies, as joint dynamics-chemistry measurements can increase the value of collected datasets and have broadening impacts (Cleary et al., 2022; Mullendore et al., 2021).

Finally, we also examine the modeled vertical NO<sub>2</sub> profiles to investigate potential challenges for satellite retrieval work which require prior vertical “shape factors” for NO<sub>2</sub> as inputs. Figure 10 shows the altitude-longitude curtains of NO<sub>2</sub> across BU (black triangle marker) and Logan Airport (red line) locations with x-w component winds. The sea-breeze cases have larger spatiotemporal variability in their NO<sub>2</sub> profiles (along with sharper spatial contrasts) compared with the non-sea-breeze cases. The plots are from the surface up to 3 km altitude, which show how the land breeze alternates with the sea breeze on different sea breeze days and impacts vertical profiles within this lower range. From 6 a.m. (not shown) to 2 p.m. LT, the westerly land breeze alternates with the low-level easterly flow after the onset of the sea breeze. By TROPOMI overpass time around 2 p.m. LT, the convergence and updraft flow near the sea breeze fronts have created steep chemical gradients in inner urban regions. In the afternoon, the varying extent of inland penetration and more aloft return flow redistribute the vertical NO<sub>2</sub> profiles from urban to suburban or rural regions. Geostationary satellites are expected to provide a unique opportunity to monitor the evolution of sea breezes across the daytime. Here we demonstrate that the spatial scale of sea breeze features in this region, together with modeling uncertainties (e.g., transport and emissions uncertainties) may pose challenges to geostationary air mass factor calculations required for satellite retrievals, and this will be explored quantitatively in separate work. Geostationary monitoring will also offer finer spatiotemporal distribution of formaldehyde (HCHO) retrievals, providing some indication of O<sub>3</sub> sensitivity by the HCHO to NO<sub>2</sub> ratio (Duncan et al., 2010; Jin et al., 2020; Martin et al., 2004), and to conduct joint inversion retrieval of NO<sub>x</sub> and volatile organic compounds (VOCs) emissions to constrain the response of ozone production to emission changes (Souri et al., 2020). The interpretation of O<sub>3</sub> chemistry from satellite-derived HCHO and NO<sub>2</sub> remains an active area of careful investigation (Johnson et al., 2022; Souri et al., 2022).

Interestingly, the relationship between peak surface concentrations and peak column abundance is complex. While surface concentrations of NO<sub>2</sub> tend to peak early in the morning (when emissions are strong and the





can increase tropospheric  $\text{NO}_2$  over suburban or rural area downwind urban emissions not currently captured by ground-based observations. We find that tropospheric  $\text{NO}_2$  can serve as an excellent indicator for monitoring sea breeze front and primary emissions.

Ozone behavior. Among the 10 sea breeze cases, available observations record 3 days when  $\text{O}_3$  exceeded 70 ppb.

We apply model process diagnostics to quantify the chemical and dynamical processes and find common quantitative features. These sea-breeze days have both efficient photochemical  $\text{O}_3$  production in the upper boundary layer (net chemical  $\text{O}_3$  production over 10 ppb/hr up to 1–2 km) and rapid  $\text{O}_3$  convergence near the surface ( $\text{O}_3$  advection tendency over 20 ppb/hr up to 300–500 m). Model results show that elevated  $\text{O}_3$  is maintained (and even worsens) when the low-level convergence zone with  $\text{O}_3$ -rich air moves to further inland regions. This may increase pollution exposure in suburban-to-rural regions even with low anthropogenic emissions. Modeled hotspots of ozone pollution hours suggest that the current network is not well-designed to represent the true importance of sea breezes on elevated  $\text{O}_3$  in the region. Sea breeze cases dominate  $\text{O}_3$  spatial heterogeneity as a result of the interactions between efficient photochemical ozone production, sea-breezes inland penetration, and uneven  $\text{NO}_x$  titration effects from urban to suburbs. It is interesting to note that while high  $\text{O}_3$  in the region may often be observed by the current network during southwesterly conditions due to the transport of pollution from upwind, our model suggests that  $\text{O}_3$  pollution over land can clearly be worse on sea breeze days but would not be identified by the observations. Many of these days begin with calm winds where  $\text{O}_3$  chemical production may be more sensitive to local emissions. To better understand the  $\text{O}_3$  behavior inland on sea breeze days and its relevance to  $\text{O}_3$  policy, future exploration of the  $\text{O}_3$  production regime would provide additional insights. The distribution of anthropogenic and biogenic VOCs emissions (model input shown in Figure S2c in Supporting Information S1) will be important to fully understand  $\text{O}_3$  chemical production in the study region. When a sea breeze front brings urban emissions into the far inland suburban-rural regions, interacting with lower- $\text{NO}_x$  and higher biogenic VOC emissions, the biogenic emissions (such as isoprene) may be expected to become important in maintaining or enhancing photochemical ozone production during the plume transport (Pfister et al., 2019). Future opportunities for this region include an evaluation of VOC emission sectors or mechanisms (e.g., marine, biogenic), and source attribution for assessing the sensitivity of  $\text{O}_3$  production to precursor emissions in urban plumes (Vermeuel et al., 2019).

*Model performance.* This work provides a new application of regional chemical transport modeling and a combination of Pandora data and multiple measurements for understanding sea breeze pollution over the Greater Boston area. High-resolution simulations at 3 km resolution are able to capture the general diurnal variations of tropospheric  $\text{NO}_2$  and urban-to-suburban differences of surface  $\text{NO}_2$  by reproducing the mesoscale sea breeze transport using HRRR 3 km as initial and boundary conditions. Anthropogenic emissions inventories impact the modeled magnitude on both column and surface  $\text{NO}_2$  but have less impact on modeled diurnal  $\text{NO}_2$  trend and  $\text{O}_3$  performance than other factors (e.g., meteorology and model uncertainties). We would like to highlight the broad range of day-to-day model performance across the sea breeze cases, and that a large bias in individual sea breeze days may contribute to an overall moderate correlation between model and long-term observations. Future opportunities for model applications include understanding model performance for retrieval in different meteorological scenarios, and increasing observation placement along sea-breeze impact region for model constraints. Furthermore, biogenic emissions emitted from urban landscapes can be associated with uncertainties arising from estimations of emission factors, urban leaf area index, and other sources (Gao et al., 2022; Kota et al., 2015). Exploration of these uncertainties and their impact on  $\text{O}_3$  air quality management over the study region could be examined in future work.

*Monitoring and satellite remote sensing implications.* The aforementioned spatiotemporal variability of air pollutants during sea breezes at this location highlights challenges and gaps in routine monitoring networks. For in-situ monitoring, additional  $\text{O}_3$  measurements at coastal and further inland hot spots could improve regional representativeness of pollution and exposure heterogeneity, provide better model constraints in the sea breeze cases, and more comprehensively identify conditions that lead to high  $\text{O}_3$ . For remote-sensing monitoring of the tropospheric  $\text{NO}_2$ , in Figure S9 in Supporting Information S1 we highlight the current monitoring capability, challenge, and observation strategies for our study area, potentially with broader implications for coastal urban regions. These include:

The polar-orbit satellites (e.g., OMI: Levelt et al., 2006, TROPOMI: Veefkind et al., 2012) have a daily overpass time around 2 p.m. LT when the sea breeze front often creates a steep gradient of tropospheric  $\text{NO}_2$  column over land. Finer pixel size, for example, from OMI at 13 km  $\times$  24 km to TROPOMI at

3.5 km × 7 km (3.5 km × 5.5 km since 6 August 2019), allows monitoring close to the urban pollution scale. However, those steep chemical gradients present in our 3 km × 3 km modeled results could pose a particular challenge in satellite monitoring with a-priori inputs on the order of 0.25-degrees or coarser. Air mass factor calculations in satellite retrievals may therefore suffer in particular from a higher error on sea breeze days due to the impact of coarse a-priori model input on the vertical NO<sub>2</sub> profile shapes (Geddes et al., 2021). In Figure S10 in Supporting Information S1 we demonstrate a preliminary comparison for averaged TCNO<sub>2</sub> in the sea breeze and non-sea breeze days between operational TROPOMI, our model result, and BU Pandora. Non-sea breeze cases have consistent TCNO<sub>2</sub> between the different approaches, while the sea breeze scenario has larger discrepancies between operational TROPOMI and modeled TCNO<sub>2</sub> in terms of magnitude and spatial distribution (e.g., model vs. TROPOMI at BU site by about a factor of 2). We know TROPOMI retrievals can be improved by higher-resolution modeling (M. Li et al., 2021; Zhao et al., 2020), and may further benefit from additional constraints from multiple well-allocated Pandoras.

The diurnal evolution of sea-breeze pollution in the coastal US regions will be captured by geostationary satellites (e.g., TEMPO at 3 km × 3 km). The standard hourly daytime measurements from the geostationary satellites will provide a unique opportunity to observe the diurnal patterns of tropospheric NO<sub>2</sub> column redistributed by the sea breeze development and various extent of inland penetration. Further opportunities exist in non-standard operations at higher time resolution comparable with Pandora observations (~5 min resolution) to monitor rapid changes in the pollutant plume. However, the spatial heterogeneity from daily to diurnal scales in the sea-breeze scenarios can add uncertainties to the air mass factor calculations for retrieval results. The variability of TCNO<sub>2</sub> within a 0.25-degree model grid box can vary by an order of magnitude during sea breezes. Taking 2 p.m. on June 28 for example, the TCNO<sub>2</sub> varies from about 0.1 DU to 1 DU, roughly a factor of 10. This is much higher with respect to roughly a factor of two in a prevailing westerly scenario. Accurate monitoring of the diurnal evolution, especially the various extents of inland penetration in the afternoon from day-to-day, is needed. The 3-km hourly model results at a similar resolution as the expected forthcoming geostationary TEMPO observations provide valuable insights for future retrieval studies.

Among other monitoring networks, Pandora instruments provide constraints on model and retrieval over the Greater Boston area. Based on our evaluation results, BU Pandora provides practical constraints in urban NO<sub>x</sub> emissions and the rapid diurnal variations of tropospheric NO<sub>2</sub> column influenced by sea breeze circulations. Combining high-resolution modeling, the accurate allocation of multiple Pandoras datasets, and other observation data provide a unique opportunity to support geostationary retrieval in the Greater Boston region.

Overall, our work provides new evidence of underestimated regional heterogeneity of O<sub>3</sub> pollution and TCNO<sub>2</sub> distribution during sea breeze development from high-resolution modeling of NO<sub>2</sub> and O<sub>3</sub> in the Greater Boston area. The spatiotemporal variability of air pollution in coastal environments, particularly during sea breezes, sets the bar higher for the representativeness of the traditional and newly developing monitoring networks in regional air quality. High-resolution information from model tools combined with well-allocated observations is required to develop customized strategies for monitoring coastal urban air quality and improving remote sensing retrieval accuracy.

### Data Availability Statement

The ambient air quality monitoring datasets are publicly available at the U.S. Environmental Protection Agency Air Quality System repository via <https://www.epa.gov/outdoor-air-quality-data>. The surface meteorological observation datasets are publicly available at the NOAA ISD Lite database via <ftp://ftp.ncdc.noaa.gov/pub/data/noaa/isd-lite/>. The AMDAR data are downloaded from <https://zenodo.org/record/3934378#.YGsWUa9Kg2z> (D. Li, 2020). The WRF-Chem preprocessor tools and emission inputs used in this study are publicly available via <https://www2.acom.ucar.edu/wrf-chem/wrf-chem-tools-community>. In addition, model output and observation data used in this analysis are freely available in the Boston University Institutional Repository, OpenBU, at: <https://open.bu.edu/handle/2144/45630>, and can also be requested by contacting the corresponding author.

**Acknowledgments**

The authors thank the two anonymous reviewers for their constructive feedback. We gratefully acknowledge that this work was funded by a NASA New Investigator Program award to project PI Jeffrey A. Geddes (80NSSC18K0745). We also acknowledge funding from NOAA Atmospheric Chemistry, Carbon Cycle and Climate Program, Grant NA20OAR4310301. The authors would like to acknowledge high-performance computing support from Cheyenne (doi: 10.5065/D6RX99HX) provided by NCAR's Computational and Information Systems Laboratory. NCAR is sponsored by the National Science Foundation (NSF). The authors also acknowledge that the data analysis work was performed on the Shared Computing Cluster which is administered by Boston University's Research Computing Services (URL: [www.bu.edu/tech/support/research/](http://www.bu.edu/tech/support/research/)). We acknowledge the use of the WRF-Chem preprocessor tools provided by the Atmospheric Chemistry Observations and Modeling Lab (ACOM) of NCAR. We thank Brian Blaylock for sharing WRF preprocessing files publicly via <https://github.com/blaylockbk> to initialize WRF simulations with HRRR boundary conditions. The authors are grateful to the Massachusetts Department of Environmental Protection and the Environmental Protection Agency for the free and public distribution of air quality monitoring data at <https://www.epa.gov/outdoor-air-quality-data>. The views, opinions, and findings contained in this work are those of the authors and should not be construed as an official position, policy, or decision.

**References**

Abdi-Oskouei, M., Carmichael, G., Christiansen, M., Ferrada, G., Roozitalab, B., Sobhani, N., et al. (2020). Sensitivity of meteorological skill to selection of wrf-chem physical parameterizations and impact on ozone prediction during the Lake Michigan ozone study (Imos). *Journal of Geophysical Research: Atmospheres*, 125(5), e2019JD031971. <https://doi.org/10.1029/2019jd031971>

Adams, T. J., Geddes, J. A., & Spinei, E. (2023). New insights into the role of atmospheric transport and mixing on column and surface concentrations of NO<sub>2</sub> at a coastal urban site. *Journal of Geophysical Research: Atmospheres*, 128, e2022JD038237. <https://doi.org/10.1029/2022JD038237>

Akbari Asanjan, A., Yang, T., Hsu, K., Sorooshian, S., Lin, J., & Peng, Q. (2018). Short-term precipitation forecast based on the persiann system and lstm recurrent neural networks. *Journal of Geophysical Research: Atmospheres*, 123(22), 12–543. <https://doi.org/10.1029/2018jd028375>

Anderson, D. C., Loughner, C. P., Diskin, G., Weinheimer, A., Canty, T. P., Salawitch, R. J., et al. (2014). Measured and modeled co and noy in discover-aq: An evaluation of emissions and chemistry over the eastern us. *Atmospheric Environment*, 96, 78–87. <https://doi.org/10.1016/j.atmosenv.2014.07.004>

Angevine, W. M., Senff, C. J., White, A. B., Williams, E. J., Koerner, J., Miller, S. T., et al. (2004). Coastal boundary layer influence on pollutant transport in New England. *Journal of Applied Meteorology and Climatology*, 43(10), 1425–1437. <https://doi.org/10.1175/jam2148.1>

Banta, R., Senff, C., Nielsen-Gammon, J., Darby, L., Ryerson, T., Alvarez, R., et al. (2005). A bad air day in houston. *Bulletin of the American Meteorological Society*, 86(5), 657–670. <https://doi.org/10.1175/bams-86-5-657>

Barbato, J. P. (1978). Areal parameters of the sea breeze and its vertical structure in the Boston basin. *Bulletin of the American Meteorological Society*, 59(11), 1420–1431. [https://doi.org/10.1175/1520-0477\(1978\)059<1420:apotsb>2.0.co;2](https://doi.org/10.1175/1520-0477(1978)059<1420:apotsb>2.0.co;2)

Barth, M., Lee, J., Hodzic, A., Pfister, G., Skamarock, W., Worden, J., et al. (2012). Thunderstorms and upper troposphere chemistry during the early stages of the 2006 North American monsoon. *Atmospheric Chemistry and Physics*, 12(22), 11003–11026. <https://doi.org/10.5194/acp-12-11003-2012>

Benjamin, S. G., Weygandt, S. S., Brown, J. M., Hu, M., Alexander, C. R., Smirnova, T. G., et al. (2016). A North American hourly assimilation and model forecast cycle: The rapid refresh. *Monthly Weather Review*, 144(4), 1669–1694. <https://doi.org/10.1175/mwr-d-15-0242.1>

Blaylock, B. K., Horel, J. D., & Crosman, E. T. (2017). Impact of lake breezes on summer ozone concentrations in the salt lake valley. *Journal of Applied Meteorology and Climatology*, 56(2), 353–370. <https://doi.org/10.1175/jamc-d-16-0216.1>

Buchholz, R., Emmons, L., Tilmes, S., & Team, T. (2019). *Cesm2.1/cam-chem instantaneous output for boundary conditions*. UCAR/NCAR-Atmospheric Chemistry Observations and Modeling Laboratory.

Caicedo, V., Delgado, R., Luke, W. T., Ren, X., Kelley, P., Stratton, P. R., et al. (2021). Observations of bay-breeze and ozone events over a marine site during the owlets-2 campaign. *Atmospheric Environment*, 263, 118669. <https://doi.org/10.1016/j.atmosenv.2021.118669>

Caicedo, V., Rappenglueck, B., Cuchiaro, G., Flynn, J., Ferrare, R., Scarino, A., et al. (2019). Bay breeze and sea breeze circulation impacts on the planetary boundary layer and air quality from an observed and modeled discover-aq Texas case study. *Journal of Geophysical Research: Atmospheres*, 124(13), 7359–7378. <https://doi.org/10.1029/2019jd030523>

Cede, A. (2017). *Manual for blick software suite 1.3 version 7 (Tech. Rep.)*. Massachusetts Department of Environmental Protection. Retrieved from [https://avdc.gsfc.nasa.gov/pub/DSCOVER/Pandora/Documents/BlickSoftwareSuite\\_Manual\\_v7.pdf](https://avdc.gsfc.nasa.gov/pub/DSCOVER/Pandora/Documents/BlickSoftwareSuite_Manual_v7.pdf)

Cleary, P. A., De Boer, G., Hupp, J. P., Borenstein, S., Hamilton, J., Kies, B., et al. (2022). Observations of the lower atmosphere from the 2021 wisodisco campaign. *Earth System Science Data*, 14(5), 2129–2145. <https://doi.org/10.5194/essd-14-2129-2022>

Colby, F. P. (2004). Simulation of the New England sea breeze: The effect of grid spacing. *Weather and Forecasting*, 19(2), 277–285. [https://doi.org/10.1175/1520-0434\(2004\)019<0277:sotnes>2.0.co;2](https://doi.org/10.1175/1520-0434(2004)019<0277:sotnes>2.0.co;2)

Darby, L. S., McKeen, S. A., Senff, C. J., White, A. B., Banta, R. M., Post, M. J., et al. (2007). Ozone differences between near-coastal and offshore sites in New England: Role of meteorology. *Journal of Geophysical Research*, 112(D16), D16S91. <https://doi.org/10.1029/2007jd008446>

Davis, W. M., Schultz, L., De C Ward, R., & Pickering, E. C. (1890). Investigations of the new England meteorological society in the year 1889. *Annals of Harvard College Observatory*, 21, 105–274.

Ding, A., Wang, T., Zhao, M., Wang, T., & Li, Z. (2004). Simulation of sea-land breezes and a discussion of their implications on the transport of air pollution during a multi-day ozone episode in the Pearl River delta of China. *Atmospheric Environment*, 38(39), 6737–6750. <https://doi.org/10.1016/j.atmosenv.2004.09.017>

Duncan, B. N., Yoshida, Y., Olson, J. R., Sillman, S., Martin, R. V., Lamsal, L., et al. (2010). Application of omi observations to a space-based indicator of nox and voc controls on surface ozone formation. *Atmospheric Environment*, 44(18), 2213–2223. <https://doi.org/10.1016/j.atmosenv.2010.03.010>

Emmons, L., Schwantes, R. H., Orlando, J. J., Tyndall, G., Kinnison, D., Lamarque, J.-F., et al. (2020). The chemistry mechanism in the community Earth system model version 2 (cesm2). *Journal of Advances in Modeling Earth Systems*, 12(4), e2019MS001882. <https://doi.org/10.1029/2019ms001882>

Fast, J. D., Gustafson, W. I., Jr., Easter, R. C., Zaveri, R. A., Barnard, J. C., Chapman, E. G., et al. (2006). Evolution of ozone, particulates, and aerosol direct radiative forcing in the vicinity of Houston using a fully coupled meteorology-chemistry-aerosol model. *Journal of Geophysical Research*, 111(D21), D21305. <https://doi.org/10.1029/2005jd006721>

Gao, Y., Ma, M., Yan, F., Su, H., Wang, S., Liao, H., et al. (2022). Impacts of biogenic emissions from urban landscapes on summer ozone and secondary organic aerosol formation in megacities. *Science of the Total Environment*, 814, 152654. <https://doi.org/10.1016/j.scitotenv.2021.152654>

Geddes, J. A., Martin, R. V., Boys, B. L., & Van Donkelaar, A. (2016). Long-term trends worldwide in ambient NO<sub>2</sub> concentrations inferred from satellite observations. *Environmental Health Perspectives*, 124(3), 281–289. <https://doi.org/10.1289/ehp.1409567>

Geddes, J. A., Wang, B., & Li, D. (2021). Ozone and nitrogen dioxide pollution in a coastal urban environment: The role of sea breezes, and implications of their representation for remote sensing of local air quality. *Journal of Geophysical Research: Atmospheres*, 126(18), e2021JD035314. <https://doi.org/10.1029/2021jd035314>

Goldberg, D. L., Lamsal, L. N., Loughner, C. P., Swartz, W. H., Lu, Z., & Streets, D. G. (2017). A high-resolution and observationally constrained omi no<sub>2</sub> satellite retrieval. *Atmospheric Chemistry and Physics*, 17(18), 11403–11421. <https://doi.org/10.5194/acp-17-11403-2017>

Grell, G. A., Peckham, S. E., Schmitz, R., McKeen, S. A., Frost, G., Skamarock, W. C., & Eder, B. (2005). Fully coupled “online” chemistry within the wrf model. *Atmospheric Environment*, 39(37), 6957–6975. <https://doi.org/10.1016/j.atmosenv.2005.04.027>

Guenther, A., Karl, T., Harley, P., Wiedinmyer, C., Palmer, P., & Geron, C. (2006). Estimates of global terrestrial isoprene emissions using Megan (model of emissions of gases and aerosols from nature). *Atmospheric Chemistry and Physics*, 6(11), 3181–3210. <https://doi.org/10.5194/acp-6-3181-2006>

- Herman, J., Cede, A., Spinei, E., Mount, G., Tzortziou, M., & Abuhassan, N. (2009). No<sub>2</sub> column amounts from ground-based Pandora and MFDOS spectrometers using the direct-sun DOAS technique: Intercomparisons and application to OMI validation. *Journal of Geophysical Research*, *114*(D13), D13307. <https://doi.org/10.1029/2009jd011848>
- Jin, X., Fiore, A., Boersma, K. F., Smedt, I. D., & Valin, L. (2020). Inferring changes in summertime surface ozone–NO<sub>x</sub>–VOC chemistry over urban areas from two decades of satellite and ground-based observations. *Environmental Science & Technology*, *54*(11), 6518–6529. <https://doi.org/10.1021/acs.est.9b07785>
- Johnson, M. S., Philip, S., Kumar, R., Naeger, A., Souri, A. H., Geddes, J., et al. (2022). Satellite remote-sensing capability to assess tropospheric column ratios of formaldehyde and nitrogen dioxide: Case study during the LISTOS 2018 field campaign. *Atmospheric Measurement Techniques Discussions*, 1–41.
- Judd, L. M., Al-Saadi, J. A., Valin, L. C., Pierce, R. B., Yang, K., Janz, S. J., et al. (2018). The dawn of geostationary air quality monitoring: Case studies from Seoul and Los Angeles. *Frontiers in Environmental Science*, *6*, 85. <https://doi.org/10.3389/fenvs.2018.00085>
- Judd, L. M., Al-Saadi, J. A., Janz, S. J., Kowalewski, M. G., Pierce, R. B., Szykman, J. J., et al. (2019). Evaluating the impact of spatial resolution on tropospheric NO<sub>2</sub> column comparisons within urban areas using high-resolution airborne data. *Atmospheric Measurement Techniques*, *12*(11), 6091–6111. <https://doi.org/10.5194/amt-12-6091-2019>
- Kim, J., Jeong, U., Ahn, M.-H., Kim, J. H., Park, R. J., Lee, H., et al. (2020). New era of air quality monitoring from space: Geostationary environment monitoring spectrometer (GEMS). *Bulletin of the American Meteorological Society*, *101*(1), E1–E22.
- Kitada, T., Igarashi, K., & Owada, M. (1986). Numerical analysis of air pollution in a combined field of land/sea breeze and mountain/valley wind. *Journal of Climate and Applied Meteorology*, *25*(6), 767–784. [https://doi.org/10.1175/1520-0450\(1986\)025<0767:naoapi>2.0.co;2](https://doi.org/10.1175/1520-0450(1986)025<0767:naoapi>2.0.co;2)
- Kota, S. H., Schade, G., Estes, M., Boyer, D., & Ying, Q. (2015). Evaluation of megan predicted biogenic isoprene emissions at urban locations in southeast Texas. *Atmospheric Environment*, *110*, 54–64. <https://doi.org/10.1016/j.atmosenv.2015.03.027>
- Kotsakis, A., Sullivan, J. T., Hanisco, T. F., Swap, R. J., Caicedo, V., Berkoff, T. A., et al. (2022). Sensitivity of total column NO<sub>2</sub> at a marine site within the Chesapeake Bay during OWLETS-2. *Atmospheric Environment*, *277*, 119063. <https://doi.org/10.1016/j.atmosenv.2022.119063>
- Levelt, P. F., Van Den Oord, G. H., Dobber, M. R., Malkki, A., Visser, H., De Vries, J., et al. (2006). The ozone monitoring instrument. *IEEE Transactions on Geoscience and Remote Sensing*, *44*(5), 1093–1101. <https://doi.org/10.1109/tgrs.2006.872333>
- Li, D. (2020). Amdar\_bl\_pblh\_dataset. [Dataset]. Zenodo. <https://doi.org/10.5281/zenodo.3934378>
- Li, J., Wang, Y., Zhang, R., Smeltzer, C., Weinheimer, A., Herman, J., et al. (2021). Comprehensive evaluations of diurnal NO<sub>2</sub> measurements during DISCOVER-AQ 2011: Effects of resolution-dependent representation of NO<sub>x</sub> emissions. *Atmospheric Chemistry and Physics*, *21*(14), 11133–11160. <https://doi.org/10.5194/acp-21-11133-2021>
- Li, M., McDonald, B., McKeen, S., Eskes, H., Levelt, P., Francoeur, C., et al. (2021). Assessment of updated fuel-based emissions inventories over the contiguous United States using TROPOMI NO<sub>2</sub> retrievals. *Journal of Geophysical Research: Atmospheres*, *126*(24), e2021JD035484. <https://doi.org/10.1029/2021jd035484>
- Loughner, C. P., Allen, D. J., Pickering, K. E., Zhang, D.-L., Shou, Y.-X., & Dickerson, R. R. (2011). Impact of fair-weather cumulus clouds and the Chesapeake Bay breeze on pollutant transport and transformation. *Atmospheric Environment*, *45*(24), 4060–4072. <https://doi.org/10.1016/j.atmosenv.2011.04.003>
- Loughner, C. P., Tzortziou, M., Follette-Cook, M., Pickering, K. E., Goldberg, D., Satam, C., et al. (2014). Impact of bay-breeze circulations on surface air quality and boundary layer export. *Journal of Applied Meteorology and Climatology*, *53*(7), 1697–1713. <https://doi.org/10.1175/jamc-d-13-0323.1>
- Mao, H., & Talbot, R. (2004). Role of meteorological processes in two New England ozone episodes during summer 2001. *Journal of Geophysical Research*, *109*(D20), D20305. <https://doi.org/10.1029/2004jd004850>
- Martin, R. V., Fiore, A. M., & Van Donkelaar, A. (2004). Space-based diagnosis of surface ozone sensitivity to anthropogenic emissions. *Geophysical Research Letters*, *31*(6). <https://doi.org/10.1029/2004gl019416>
- Martins, D., Stauffer, R., Thompson, A., Knepp, T., & Pippin, M. (2012). Surface ozone at a coastal suburban site in 2009 and 2010: Relationships to chemical and meteorological processes. *Journal of Geophysical Research*, *117*(D5). <https://doi.org/10.1029/2011jd016828>
- Massachusetts 2019. (2020). *Air quality report (Tech. Rep.)*. Massachusetts Department of Environmental Protection. Retrieved from <https://www.mass.gov/doc/2019-annual-air-quality-report>
- McDonald, B. C., McKeen, S. A., Cui, Y. Y., Ahmadov, R., Kim, S.-W., Frost, G. J., et al. (2018). Modeling ozone in the eastern US using a fuel-based mobile source emissions inventory. *Environmental Science & Technology*, *52*(13), 7360–7370. <https://doi.org/10.1021/acs.est.8b00778>
- Miller, S., Keim, B., Talbot, R., & Mao, H. (2003). Sea breeze: Structure, forecasting, and impacts. *Reviews of Geophysics*, *41*(3), 1011. <https://doi.org/10.1029/2003rg000124>
- Mullendore, G. L., Barth, M. C., Klein, P. M., & Crawford, J. H. (2021). Broadening impact of field campaigns: Integrating meteorological and chemical observations. *Bulletin of the American Meteorological Society*, *102*(3), E464–E475. <https://doi.org/10.1175/bams-d-19-0216.1>
- Pfister, G., Wang, C.-T., Barth, M., Flocke, F., Vizuete, W., & Walters, S. (2019). Chemical characteristics and ozone production in the northern Colorado front range. *Journal of Geophysical Research: Atmospheres*, *124*(23), 13397–13419. <https://doi.org/10.1029/2019jd030544>
- Rieder, H. E., Fiore, A. M., Horowitz, L. W., & Naik, V. (2015). Projecting policy-relevant metrics for high summertime ozone pollution events over the eastern United States due to climate and emission changes during the 21st century. *Journal of Geophysical Research: Atmospheres*, *120*(2), 784–800. <https://doi.org/10.1002/2014jd022303>
- Souri, A. H., Choi, Y., Jeon, W., Li, X., Pan, S., Diao, L., & Westenbarger, D. A. (2016). Constraining NO<sub>x</sub> emissions using satellite NO<sub>2</sub> measurements during 2013 DISCOVER-AQ Texas campaign. *Atmospheric Environment*, *131*, 371–381. <https://doi.org/10.1016/j.atmosenv.2016.02.020>
- Souri, A. H., Johnson, M. S., Wolfe, G. M., Crawford, J. H., Fried, A., Wisthaler, A., et al. (2022). Characterization of errors in satellite-based hCHO/NO<sub>2</sub> tropospheric column ratios with respect to chemistry, column to PBL translation, spatial representation, and retrieval uncertainties. *Atmospheric Chemistry and Physics Discussions*, 1–43.
- Souri, A. H., Nowlan, C. R., González Abad, G., Zhu, L., Blake, D. R., Fried, A., et al. (2020). An inversion of NO<sub>x</sub> and non-methane volatile organic compound (NMVOC) emissions using satellite observations during the KORUS-AQ campaign and implications for surface ozone over East Asia. *Atmospheric Chemistry and Physics*, *20*(16), 9837–9854. <https://doi.org/10.5194/acp-20-9837-2020>
- Stanier, C. O., Pierce, R. B., Abdi-Oskouei, M., Adelman, Z. E., Al-Saadi, J., Alwe, H. D., et al. (2021). Overview of the Lake Michigan ozone study 2017. *Bulletin of the American Meteorological Society*, *102*(12), E2207–E2225. <https://doi.org/10.1175/bams-d-20-0061.1>
- Stauffer, R. M., Thompson, A. M., Martins, D. K., Clark, R. D., Goldberg, D. L., Loughner, C. P., et al. (2015). Bay breeze influence on surface ozone at Edgewood, MD during July 2011. *Journal of Atmospheric Chemistry*, *72*(3), 335–353. <https://doi.org/10.1007/s10874-012-9241-6>
- Sullivan, J. T., Berkoff, T., Gronoff, G., Knepp, T., Pippin, M., Allen, D., et al. (2019). The ozone water-land environmental transition study: An innovative strategy for understanding Chesapeake Bay pollution events. *Bulletin of the American Meteorological Society*, *100*(2), 291–306. <https://doi.org/10.1175/bams-d-18-0025.1>

- Thompson, A. M., Stauffer, R. M., Boyle, T. P., Kollonige, D. E., Miyazaki, K., Tzortziou, M., et al. (2019). Comparison of near-surface no<sub>2</sub> pollution with pandora total column no<sub>2</sub> during the korea-United States ocean color (korus oc) campaign. *Journal of Geophysical Research: Atmospheres*, *124*(23), 13560–13575. <https://doi.org/10.1029/2019jd030765>
- Travis, K. R., Jacob, D. J., Fisher, J. A., Kim, P. S., Marais, E. A., Zhu, L., et al. (2016). Why do models overestimate surface ozone in the south-east United States? *Atmospheric Chemistry and Physics*, *16*(21), 13561–13577. <https://doi.org/10.5194/acp-16-13561-2016>
- Veeffkind, J., Aben, I., McMullan, K., Förster, H., De Vries, J., Otter, G., et al. (2012). Tropomi on the esa sentinel-5 precursor: A gmes mission for global observations of the atmospheric composition for climate, air quality and ozone layer applications. *Remote sensing of environment*, *120*, 70–83. <https://doi.org/10.1016/j.rse.2011.09.027>
- Vermeuel, M. P., Novak, G. A., Alwe, H. D., Hughes, D. D., Kaleel, R., Dickens, A. F., et al. (2019). Sensitivity of ozone production to nox and voc along the lake Michigan coastline. *Journal of Geophysical Research: Atmospheres*, *124*(20), 10989–11006. <https://doi.org/10.1029/2019jd030842>
- Wentworth, G., Murphy, J., & Sills, D. (2015). Impact of lake breezes on ozone and nitrogen oxides in the greater Toronto area. *Atmospheric Environment*, *109*, 52–60. <https://doi.org/10.1016/j.atmosenv.2015.03.002>
- Wiedinmyer, C., Akagi, S., Yokelson, R. J., Emmons, L., Al-Saadi, J., Orlando, J., & Soja, A. (2011). The fire inventory from near (finn): A high resolution global model to estimate the emissions from open burning. *Geoscientific Model Development*, *4*(3), 625–641. <https://doi.org/10.5194/gmd-4-625-2011>
- Wong, J., Barth, M., & Noone, D. (2013). Evaluating a lightning parameterization based on cloud-top height for mesoscale numerical model simulations. *Geoscientific Model Development*, *6*(2), 429–443. <https://doi.org/10.5194/gmd-6-429-2013>
- Zhang, J., Ninneman, M., Joseph, E., Schwab, M. J., Shrestha, B., & Schwab, J. J. (2020). Mobile laboratory measurements of high surface ozone levels and spatial heterogeneity during listas 2018: Evidence for sea breeze influence. *Journal of Geophysical Research: Atmospheres*, *125*(11), e2019JD031961. <https://doi.org/10.1029/2019jd031961>
- Zhang, Y., Li, D., Lin, Z., Santanello, J. A., Jr., & Gao, Z. (2019). Development and evaluation of a long-term data record of planetary boundary layer profiles from aircraft meteorological reports. *Journal of Geophysical Research: Atmospheres*, *124*(4), 2008–2030. <https://doi.org/10.1029/2018jd029529>
- Zhao, X., Griffin, D., Fioletov, V., McLinden, C., Cede, A., Tiefengraber, M., et al. (2020). Assessment of the quality of tropomi high-spatial-resolution no<sub>2</sub> data products in the greater toronto area. *Atmospheric Measurement Techniques*, *13*(4), 2131–2159. <https://doi.org/10.5194/amt-13-2131-2020>
- Zoogman, P., Liu, X., Suleiman, R., Pennington, W., Flittner, D., Al-Saadi, J., et al. (2017). Tropospheric emissions: Monitoring of pollution (tempo). *Journal of Quantitative Spectroscopy and Radiative Transfer*, *186*, 17–39. <https://doi.org/10.1016/j.jqsrt.2016.05.008>